TECHNISCHE UNIVERSITÄT WIEN
Vienna University of Technology

Master Thesis

Simulation of a Fluidized Bed Regenerative Heat Exchanger

Ing. Felix Birkelbach, BSc

1026754

at the

Institute for Energy Systems and Thermodynamics

supervised by

Ao.Univ.Prof. Dipl.-Ing. Dr.techn. Andreas Werner

Univ.Ass. Dipl.-Ing. Karl Schaiger, BSc

Vienna, August 15, 2016

Abstract

Due to increasing awareness and recent legislation heat recovery is becoming more and more important, in an effort to increase energy efficiency. Especially in energy intensive industries like iron and steel production, numerous high-temperature excess heat sources are available that can be used to produce electricity, if no heat sinks are available to use the heat directly. Steam cycles offer efficient means to convert the heat into electricity, but they require continuous heat supply to avoid thermal stress and dilatation issues within the turbine. If no additional heat sources are to be used, an appliance to buffer the discontinuous excess heat is required to smooth the temperature profile.

In this thesis the application of a fluidized-bed heat regenerator in the heat recovery from a steel casting process is investigated. A Matlab model has been developed and the influence of a range of construction parameters on the capacity to smooth the temperature profile and the efficiency of the regenerator was investigated to point out optimization potentials. Furthermore the effect of reversing the flow direction of the heat transfer medium during discharging is analyzed.

Overall the simulation results suggest that it should be possible to build a regenerator that reduces the temperature variation of the working medium from 85 K to 11 K at a heat transfer medium mass flow of 12 kg/s in a process with a cycle duration of 1 h and a duty cycle of 3:1. The regenerator would have a size of 14 m×3 m×3.5 m, contain 92 t particles with a mean diameter of 80 µm and tubes with a total surface area of 440 m^2. This regenerator would transfer 650 kWh with a thermal efficiency of approximately 90 %.

Especially the high capacity and thermal efficiency should make this technology very attractive in heat recovery applications, though it remains to be seen if these values can actually be achieved in real-world regenerators. Regardless, further development, e.g. regarding a control mechanism, could reduce the size and material requirement of the regenerator further to increase the competitiveness of the fluidized-bed heat regenerator compared to other technologies.

Acknowledgments

First I would like to thank Andreas Werner for supervising my thesis, for his continuing support throughout the writing process and for his valuable feedback, that helped shape my thesis.

Equally I would like to thank Karl Schwaiger for his guidance in the beginning, when I did not quite know where to start, for his willingness to always discuss the questions that I had, regardless of how particular they were, as well as his patience in doing so.

Also I would like to thank Florian Wesenauer for providing me with a preliminary version of his work on heat transfer coefficients in fluidized beds so I could read up on that before the work was officially published.

On a completely different matter I would like to thank my parents. Namely, that they allowed me to return back home when the writing started to become intense. There is nothing like the comfort and isolation of your parents' place when you need to get work done for your thesis.

And last but not least I would like to thank all my friends who proof-read my thesis. It is astonishing how many errors other people find in your work even after you proof-read it yourself multiple times.

Thank you!

Contents

1 Introduction

In recent years the pressure on companies to implement energy efficiency measures has increased significantly. It is not just NGOs anymore that are pushing for the improvement of environmental standards but also legislative authorities all over the world releasing new laws with the aim to regulate the industries environmental footprint. Growing concern for global warming has led the EU to release the directive 2012/27/EU on energy efficiency which, among other regulations, requires big companies to implement energy efficiency measures and undergo regular audits by independent auditors. This directive has been implemented into Austrian law as the Bundes-Energieeffizienzgesetz (BGBl. I Nr. 72/2014). As the the largest emitter of CO_2 in the manufacturing sector (30 % globally, International Energy Organization 2010, p. 165), the iron and steel industry is strongly affected by this recent legislation.

As a guideline the EU has published a reference document for best practices in the iron and steel production industry (ISP BAT) and another one for the ferrous metal processing industry (FMP BAT). These documents provide an overview over established technologies for reducing the environmental footprint in general and also describe technologies for improving the energy efficiency in particular. All energy efficiency measures are aimed at reducing the consumption of primary energy like electricity or natural gas with the ultimate goal of reducing carbon dioxide and other emissions to curb global warming and pollution. The IEA estimates that the implementation of the measures described in the above mentioned documents in existing steel mills could reduce the use of primary energy in the iron and steel industry by as much as 22 % and the emissions of CO_2 by 19 % annually (International Energy Organization 2010, p. 165). Despite the wide range of available technologies there is a lot of effort being made to develop cheaper and more efficient ones.

One important target of energy efficiency measures is the recovery of excess heat[1]. Many manufacturing steps in the steel industry have to be done at high temperatures in order to make the material processable or for certain chemical reactions to take place. When the processing is done the material remains hot and without further measures this heat would be lost. In other processes, e.g. quenching, the material is cooled from high temperatures very quickly to achieve certain properties like increased hardness. The heat that is released this way should also be recovered.

Yet the realization of efficient heat recovery measures is not a trivial endeavour. Numerous problems regarding the development of specialized appliances and the implementation into existing processes have to be solved. If no additional external heat source is used there typically are two central problems from a thermodynamic perspective: For one the

[1] In the literature the terms excess heat and waste heat, sometimes also surplus heat, are used interchangeably. While the heat might be waste for the process that produces it, it is anything but that from a system point of view. It can be utilized effectively in other processes with the right technology. Therefore I will use the term excess heat throughout this work, to emphasize that this heat is not waste at all.

temperature level of the heat is usually defined by the process that produces the excess heat and the process that uses the excess heat has to be specially designed to work at this specific temperature level. Also excess heat supply is typically discontinuous, which requires the process that uses the excess heat to either switch between different load conditions frequently or a technology to buffer heat in order to smooth the temperature profile.

Components that passively buffer heat in a process with alternating cycles of heat supply and demand are usually referred to as regenerators. In principle a regenerator is a type of heat exchanger that is combined with heat storage. While pure heat exchangers have two separate fluid systems for the hot and the cold medium and operate continuously, one of these fluid systems is replaced by a heat storage in regenerators. A regenerator stores heat when a hot heat transfer medium is flowing through its channels and releases heat when the cold medium is flowing. If the hot and the cold medium are the same medium with varying temperature the regenerator smooths the temperature profile of the heat transfer medium. If different media are used heat can be transferred from one medium to the other with intermediate storage. In the latter form regenerators are already widely used in the steel industry for preheating the combustion air in blast furnaces. The heat from the flue gas is alternatingly stored in and recovered from a number of firebrick lined vessels. The result of this preheating is a considerable reduction of primary fuel demand for the furnace. This technology is known as hot blast and it is considered one of the most important advances in the iron industry during the industrial revolution. More modern furnace regenerators use fixed beds of ceramic balls to store the heat (FMP BAT, chapter D1.1).

If there is no immediate demand for the excess heat, like for preheating in a blast furnace, it is usually converted to electricity. Johansson et al. 2014 provides a discussion of different conversion methods for the application in the steel industry and their viability. She concludes that organic rankine cycles are best suited for temperatures above 90 °C and confirms their economic viability. For temperatures above 200 °C steam can also be used as a working medium in the rankine cycle. Compared to cycles with organic working media, steam cycles typically feature a higher efficiency but they are much more sensitive to discontinuous load conditions (Campana et al. 2013).

Provided that an excess heat source exists in a sufficiently high temperature range a steam cycle would be the most efficient means to convert that heat into electricity from a thermodynamic point of view, even though that requires a heat buffer in addition. Since the decision to implement a certain technology is always also an economic one, the additional costs compared to an organic rankine cycle may not exceed the efficiency benefits. While the components for the steam cycle are already well-developed and can be bought from a range of suppliers, the development of industrial scale regenerators is still in its infancy. Therefore the break through of steam cycles in heat recovery applications will be significantly influenced by the availability of an efficient, reliable and affordable regenerator that ensures continuous heat supply to the turbine. A fluidized bed regenerator might fulfill all these requirements.

2 Scope of Work

The aim of the present work is to assess the applicability of a fluidized bed regenerator as a heat buffer in a steam cycle that is driven by the excess heat from a slab casting process and to determine the effect of certain design parameters on its performance.

In a slab casting process heat can be recovered for about 45 minutes from a hot iron slab with a working medium temperature of around 450 °C. For the downstream superheated steam turbine to work correctly the input temperature has to stay within a narrow interval of ±5 K, otherwise thermal stress and dilatation issues might arise. Therefore the heat has to be provided by the regenerator to stabilize the temperature in the following 15 minutes in which no hot slab is available. Similarly to the ceramic ball regenerator for blast furnaces (ISP BAT) granular bed technology could provide efficient means to accomplish this task.

In granular beds the solid granular material that makes up the bed is brought in contact with a fluid that flows through the cavities of the bed. The main advantage of granular beds is the high specific surface area of the particles, which enables rapid interaction between fluid and solid. Once the superficial velocity of the fluid (fluidization velocity) exceeds the minimum fluidization velocity, a characteristic value of a bed under specific operating conditions, the solid particles start behaving like a fluid. Depending on whether the fluid velocity is below or above the minimum fluidization velocity, the bed is referred to as fixed/packed bed or fluidized bed respectively. A fluidized bed benefits from rapid particle mixing which leads to near constant operating conditions across the whole bed. The technology has its origin in the chemical industry where it is used to ensure rapid homogeneous gas-solid reactions among a vast number of other applications.

In heat storage applications the bed material acts as the heat storage material and by controlling the fluidization velocity the heat transfer conditions can be controlled. Regenerators utilizing granular bed technology can be distinguished by considering three features:

1. Whether or not the heat transfer medium comes into contact with the bed material. In some applications (e.g. ceramic beds for hot blast described above) the heat transfer medium (in that case the flue gas) is blown directly through the bed, i.e. the heat transfer medium also acts as fluidization medium. In other applications, like the one that is covered in this work, the working medium (steam) flows through tubes that are immersed in the bed while dry air is used as fluidization medium. This way the steam never comes in contact with the bed material.

2. The deployed bed material. Most importantly if the heat is stored as latent heat in phase change materials or if it is stored as sensible heat, e.g. in sand like in this thesis. Phase change materials, usually molten slat, feature a higher effective volumetric heat capacity, because a high share of the heat is stored as melting enthalpy, resulting in more compact installations. Sand on the other hand is a low

cost material and less prone to wear (Izquierdo-Barrientos et al. 2013) making the bed more durable and cost-efficient.

3. The fluidization regime that the bed operates in. The bed may operate as a fixed bed or fluidized bed depending on the velocity of the gas flowing through the bed as described above. In the application covered in the present work the bed is fluidized because it enables more dynamic operation due to the increased heat conductivity between the bed and the immersed tubes and the rapid heat propagation within the bed.

For the application at an industrial scale, the regenerator has to feature a sufficient heat capacity to buffer the heat and rapid heat transfer for dynamic operation while at the same time being as compact as possible. All these requirements must be met at low cost and with acceptable efficiency to justify the implementation of this heat recovery mechanism.

To analyze the influence of design parameters on the above mentioned criteria a simulation model for the regenerator has been developed. It models the heat transfer from the heat transfer medium to the bed dynamically and also takes the fluidization conditions of the bed into account. Multiple simulation runs with different parameter settings under quasi-static conditions have been performed to obtain the data for the analysis. Specifically the influence of the fluidization conditions, particle size, dynamic factor (the ratio of the process time constant to the thermal time constant of the regenerator) and the geometry of the regenerator setup have been investigated.

Usually the temperature across the bed is assumed to be constant ("Ideal stirred tank"). This implies that the heat propagation within the bed is infinitely fast. To investigate the influence of finite heat transfer a cell model has been developed that models the heat transfer within the fluidized bed depending on the fluidization conditions and the results have been compared to the ones of the ideal model.

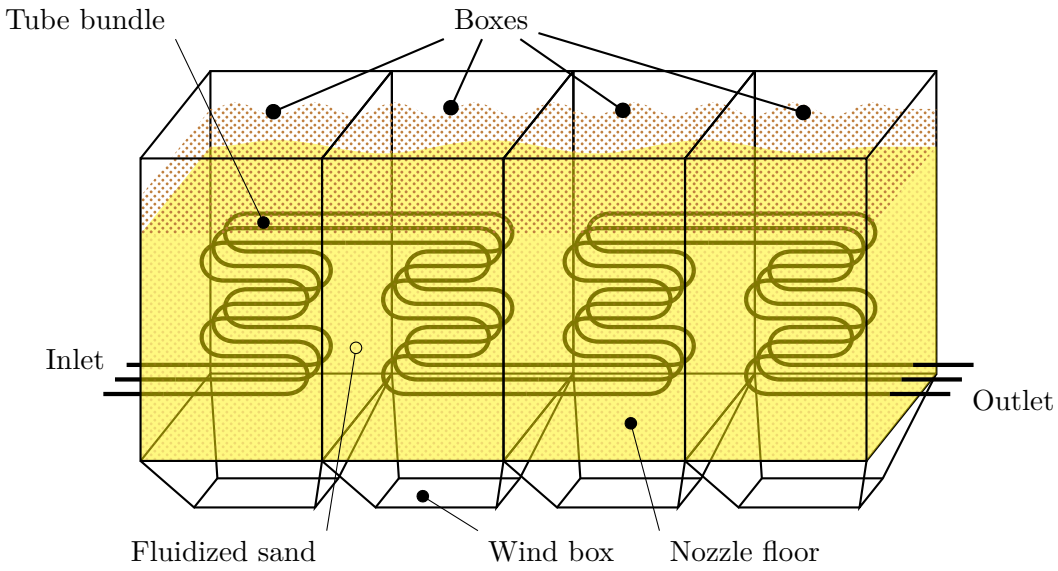

Figure 1: Sketch of a regenerator setup

3 Modeling of the Regenerator

The aim of the modeling is to find a mathematical representation of the real world regenerator that allows to draw conclusions on the regenerator's functioning by running simulations. It has to be defined which type of regenerator is to be modeled and which physical processes are to be considered to what degree. The model should cover a wide range of regenerator configurations and consider all relevant physical processes without being overly complex. It also has to capture all relevant parameters that describe the boundary conditions, the configuration of the regenerator and the physical process within the regenerator and group these parameters in a concise way. To link the parameters and describe the functioning of the regenerator suitable formulas have to be included.

3.1 Regenerator setup

The fluidized bed regenerator, considered in the present work, consists of an array of fluidized beds which are connected in series. Figure 1 shows a setup with four boxes. Each fluidized bed operates independently from the other fluidized beds and the fluidization parameters are chosen so that the fluidized bed operates close to its minimum fluidization point. That way the energy loss, caused by the entalpy flow in the fluidization medium that flows through the bed, and the work that is required to compress the fluidization medium are kept as low as possible, while at the same time utilizing the advantages of the increased heat transfer in the fluidized regime. In order to achieve good fluidization at low fluidization velocities very small grained particles in the range of 80 µm to 120 µm particle diameter are used as bed material.

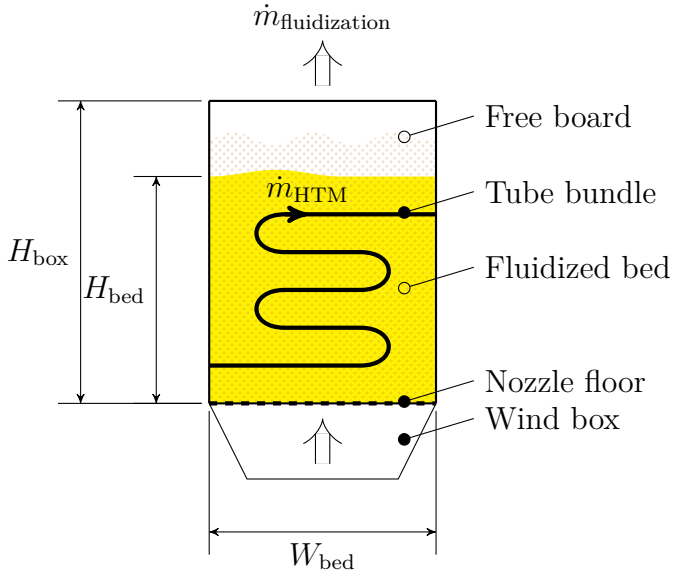

Figure 2: Sketch of a fluidized bed

The fluidization medium, in this case dry air, flows through the wind box and then enters the bed through the nozzle floor. The nozzle floor ensures homogeneous distribution of the fluidization medium across the base area of the bed. Also it prevents the bed particles from entering the wind box. After exiting the bed the fluidization medium is recirculated.

The heat transfer medium (working medium from the point of view of the steam cycle) flows through a tube bundle which makes a couple of turns in each box to increase the surface area for the heat exchange. Figure 1 shows a tube bundle with three tubes and four turns in each box.

3.2 Modeling of the fluidized bed

Each fluidized bed (see figure 2) is housed in a box, which is assumed to be surrounded by adiabatic walls. Heat is only transported through the tube bundle that is immersed in the bed and through the fluidization medium, that enters the bed through the nozzle floor and exits at the top of the box.

One of the key parameters describing the operation mode of a (fluidized) bed is the fluidization ratio. It is defined as the ratio of the superficial gas velocity u, i.e. the velocity of the fluidization medium if the bed particles would not be present, to the minimum fluidization velocity u_{mf}. The minimum fluidization velocity is the velocity at which the bed particles start acting as if they were a fluid.

Figure 3 shows the different fluidization regimes in a normalized pressure drop vs. fluidization ratio diagram to illustrate the two regimes. In the Handbook of Fluidization

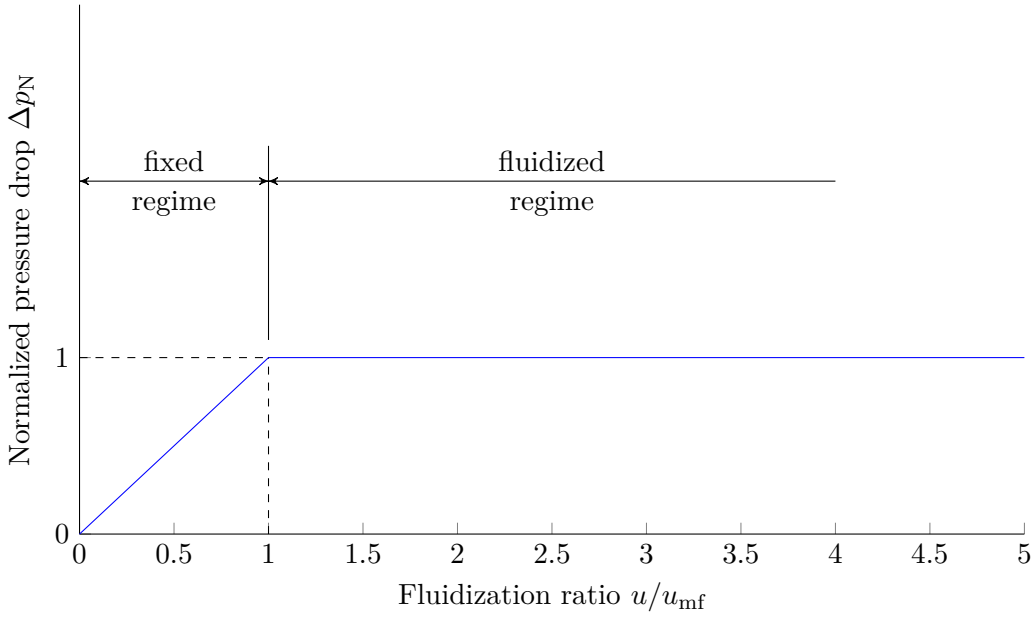

Figure 3: Classification of fluidization regimes

the normalized pressure drop across the bed Δp_N is defined as

$$\Delta p_N = \frac{\Delta p A_{bed}}{g m_{bed}} \frac{\rho_{particle}}{\rho_{particle} - \rho_{fluid}} \tag{1}$$

where Δp is the real pressure drop, A_{bed} is the base area of the bed, g is the gravity constant and m_{bed} denotes the particle mass.

For fluidization velocities smaller than the minimum fluidization velocity the bed is referred to as a fixed (or packed) bed. The pressure drop across the bed increases proportionally to the fluidization velocity. Starting from u_{mf} the bed starts behaving like a fluid and the pressure drop remains approximately constant (until the terminal velocity u_T is reached and the fluidized bed enters the circulating regime — but this regime is not of relevance for thermal storage applications).

Once the fluidization velocity exceeds the minimum fluidization velocity the heat transfer coefficient between the then fluidized bed and the immersed tube bundle features a sharp increase. This increase is crucial to the viability of this technology because it enables the high heat transfer rates required for dynamic operation. Also the heat propagation within the bed is increased due to the free movement and mixing of particles. Even though these two effects would suggest that selecting a high fluidization velocity would be a good idea, the fluidization velocity cannot be increased at will since it also increases the energy loss and thereby adversely affects the energetic efficiency of the regenerator.

In addition to the parameters that describe the setup of the bed, models for three different processes are required to describe the behavior of a fluidized bed.

Fluidization model: Describes the expansion state of the bed.

Temperature model: Describes the temperature distribution in the fluidized bed.

Tube-bed conductivity model: Describes the heat transfer between the bed and the immersed tubes.

Even though each of these models requires information from the other two, models of the same type should be interchangeable. E.g. the fluidization model should compute the bed expansion correctly regardless of whether the bed temperature is computed with the ideal stirred tank or the diffusion model.

The following sections give a description of all implemented models.

3.2.1 Fluidization model: Linear

Gas-solid-beds usually do not exhibit homogeneous fluidization. Instead most of the fluidization medium passes through the bed in bubbles. Beds with fine grained particles, such as the one considered here, start bubbling almost immediately after entering the fluidized regime. Therefore the bed expansion Ψ would have to be estimated with the two-phase theory. But since no significant influence on this simulation is expected it has been estimated with the linear model from chapter M5 in the VDI-heat-atlas for the sake of simplicity.

$$\Psi = 1 - \frac{V_{\text{particles}}}{V_{\text{bed}}} \approx \Psi_{\text{mf}} + (1 - \Psi_{\text{mf}}) \frac{u - u_{\text{mf}}}{u_{\text{T}} - u_{\text{mf}}} \tag{2}$$

with the minimum fluidization velocity u_{mf} and the terminal velocity u_{T}:

$$\frac{u_{\text{mf}} d_{\text{P}}}{\nu_{\text{fluid}}} = 42.9(1 - \Psi_{\text{mf}}) \left(\sqrt{1 + \frac{\Psi_{\text{mf}}^3}{(1 - \Psi_{\text{mf}})^2} \frac{\text{Ar}}{3214}} - 1 \right) \tag{3}$$

$$\frac{u_{\text{T}} d_{\text{P}}}{\nu_{\text{fluid}}} = \sqrt{\frac{4}{3} \text{Ar}} \tag{4}$$

Ψ_{mf} is the bed expansion at $u = u_{\text{mf}}$ and is a characteristic value of the utilized bed material. d_{p} is the mean particle diameter, ν_{fluid} the dynamic viscosity of the fluid and Ar the Archimedes number:

$$\text{Ar} = \frac{(\rho_{\text{particle}} - \rho_{\text{fluid}}) g d_{\text{P}}^3}{\rho_{\text{fluid}} \nu_{\text{fluid}}^2} \tag{5}$$

Knowing the bed expansion, the bed height H_{bed} can be calculated with

$$H_{\text{bed}} = \frac{m_{\text{bed}}}{\rho_{\text{particle}} (1 - \Psi) A_{\text{bed}}} \tag{6}$$

3.2.2 Temperature model: Ideal stirred tank

This model assumes, that the particle temperature is constant across the whole bed. All mixing and diffusion processes take place on a timescale much smaller than the simulation timescale and can therefore be neglected. This assumption simplifies the calculations a lot. Instead of the partial differential equation that describes heat conduction in the general case only an first-order ordinary differential equation has to be solved. Also the bed temperature can be represented by one single value instead of a scalar field.

The governing differential equation is

$$m_{\mathrm{bed}} c_{p,\mathrm{particle}} \frac{\partial T_{\mathrm{bed}}}{\partial \mathrm{t}} = \dot{Q} \tag{7}$$

Simple forward discretization leads to an explicit Euler-Scheme

$$T_{\mathrm{bed}}^{i+1} = T_{\mathrm{bed}}^{i} + \dot{Q}^{i} \frac{\Delta t}{c_{p,\mathrm{particle}}^{i} m_{\mathrm{bed}}} \tag{8}$$

The heat flow $\dot{Q}^i$ in equation (8) represents the total heat flow from the tubes to the bed and the energy loss due to the entalpy flow in the fluidization medium at the timestep i. Assuming that the fluid enters with the temperature $T_{\mathrm{fluid,in}}^{i}$, which is given, and exits with the bed temperature $T_{\mathrm{fluid,out}}^{i} = T_{\mathrm{bed}}^{i}$:

$$\dot{Q}^{i} = \sum \dot{Q}_{\mathrm{bed}}^{i} + \left[(T c_p)_{\mathrm{fluid,in}}^{i} - (T c_p)_{\mathrm{fluid,out}}^{i} \right] \dot{m}^{i} \tag{9}$$

3.2.3 Temperature model: Diffusion

The ideal stirred tank model tends to overestimate the heat transferred between the tubes and the bed because it does not take into account potential local overheating due to finite temperature propagation within the bed. Especially at low fluidization ratios this might become a limiting factor.

Heat transfer within the fluidized bed is dominated by heat transfer due to particle mixing and heat transported by the fluidization medium. Conduction between particles and radiation play only a subordinate role. Since the fluid dynamic processes determining the particle flow are extremely complex a more simplistic model that only models the effective heat flow due to particle mixing will be employed.

The governing differential equation for a differentially small volume element is

$$\frac{m_{\mathrm{bed}}}{V_{\mathrm{bed}}} c_{p,\mathrm{particle}} \frac{\partial T_{\mathrm{bed}}}{\partial \mathrm{t}} = \dot{q} + \nabla \left(\begin{bmatrix} k_x & 0 \\ 0 & k_y \end{bmatrix} \nabla T_{\mathrm{bed}} \right) \tag{10}$$

with k_{x} and k_{y} being the effective heat conductivity due to the mixing of particles and conduction through the particles in x and y direction respectively. Since the effect

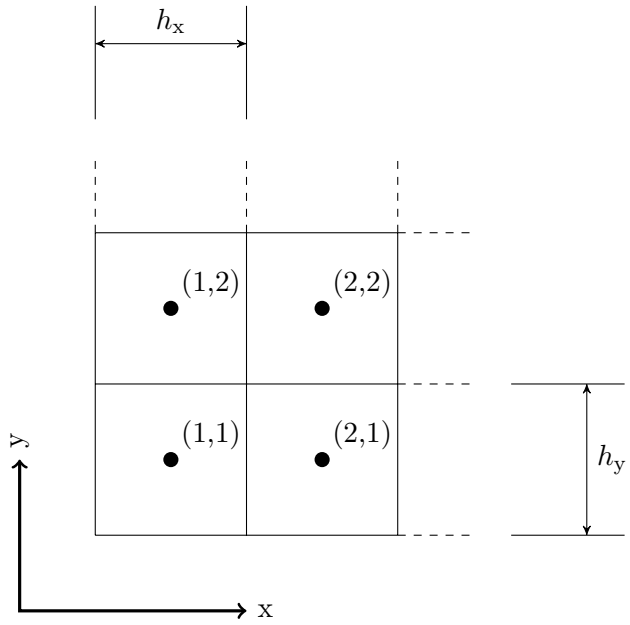

Figure 4: Sketch of the grid used for discetizing the heat transfer equation

of particle mixing is by orders of magnitude higher than the conduction through the particles in a fluidized bed the latter is neglected.

The heat transfer equation has been discretized in space using the finite volume method. This method has the advantage of fulfilling the energy balance for each cell and therefore also globally. The result is a system of first order ordinary differential equations in time. Since this system is generally a stiff problem a specialized MatLab ODE-solver has been used instead of manually discretizing the equation in the time-domain.

The discretization has been done on a equally spaced anisotropic rectangular grid (see figure 4) with N_x and N_y cells in x and y direction respectively. The nodes are placed in the center of each cell so that

$$T_{j,k}(t) \simeq T_\mathrm{bed}(x_j, y_k, t)$$

with

$$x_j = h_\mathrm{x}\left(j - \frac{1}{2}\right) \qquad y_k = h_\mathrm{y}\left(k - \frac{1}{2}\right)$$
$$h_\mathrm{x} = \frac{W_\mathrm{bed}}{N_\mathrm{x}} \qquad h_\mathrm{y} = \frac{H_\mathrm{bed}}{N_\mathrm{y}}$$

Integration over each cell and subsequent manipulation leads to the discrete scheme

$$\frac{\partial T}{\partial \mathrm{t}} \simeq \frac{V_{j,k}}{m_{j,k}c_{p,j,k}}\left[\frac{\dot{Q}_{j,k}}{V_{j,k}} + k_\mathrm{y}\frac{T_{j,k-1} - 2T_{j,k} + T_{j,k+1}}{h_\mathrm{y}^2} + k_\mathrm{x}\frac{T_{j-1,k} - 2T_{j,k} + T_{j+1,k}}{h_\mathrm{x}^2}\right] \qquad (11)$$

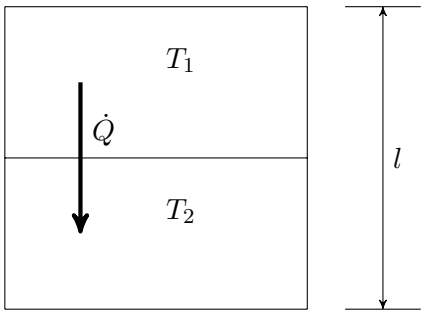

Figure 5: Sketch of the two cell diffusion model

of second order accuracy. Similarly to equation (9) the $\dot{Q}_{j,k}$ terms take both the tube-bed heat flow and the energy loss due to the entalpy flow in fluidization medium into account.

Since the walls of the box containing the bed are assumed to be adiabatic, no-flow boundary conditions have been applied along the border. The heat that is extracted from the bed by the fluidization medium that passes through the bed is included in $\dot{Q}_{j,k}$.

There are numerous works that analyze the mixing behavior of the particles in fluidized beds. Some of them, e.g. Mostafazadeh et al. 2013, use the axial and lateral particle velocities to describe the mixing behavior. Others, e.g. Luo et al. 2015, derive a dispersion parameter. Both of these approaches cannot be integrated directly into this temperature model. Instead the effective heat transfer coefficients for this model have been estimated via the bed turnover time. This value is defined as the time it takes to completely "mix" a bed under certain operating conditions.

In chapter 12.1.3 of the Handbook of Fluidization an empirical correlation for the bed turnover time t_T is given:

$$t_\mathrm{T} = \frac{H_\mathrm{bed}}{Y(u - u_\mathrm{mf})(\beta_\mathrm{w} + 0.38\beta_\mathrm{d})} \tag{12}$$

with the bed height H_bed, and the dimensionless constants Y, β_w and β_d which are given in the form of diagrams. For the present work the values $Y = 0.8$, $\beta_\mathrm{w} = 0.4$ and $\beta_\mathrm{d} = 1$ were used.

Now a formula to link the heat transfer coefficient with the bed turnover time needs to be derived. In a two cell model (figure 5) the temperature over time, when bringing two cells with different initial temperatures $T_{1,0}$ and $T_{2,0}$ in contact, can be calculated analytically.

Solving the system of differential equations

$$\begin{bmatrix} \frac{\partial T_1}{\partial \mathrm{t}} \\ \frac{\partial T_2}{\partial \mathrm{t}} \end{bmatrix} = \frac{kl}{2mc_p} \begin{bmatrix} -1 & 1 \\ 1 & -1 \end{bmatrix} \begin{bmatrix} T_1 \\ T_2 \end{bmatrix} \tag{13}$$

leads to

$$\begin{bmatrix} T_1(t) \\ T_2(t) \end{bmatrix} = \frac{T_{1,0} + T_{2,0}}{2} + \frac{T_{1,0} - T_{2,0}}{2} \begin{bmatrix} 1 \\ -1 \end{bmatrix} \exp\left(-\frac{kl}{mc_p} t \right) \tag{14}$$

Assuming that the turnover time is the time it takes to reach thermal equilibrium, that is when the argument of the exponential function in (14) is about to -4, the horizontal heat conductivity can be estimated with

$$k_x = \frac{4 m_{\mathrm{cell}} c_{p,\mathrm{particle}}}{t_{\mathrm{T}} W_{\mathrm{bed}}} \tag{15}$$

and analogously for the vertical heat conductivity.

It is easy to see that $k \propto (u - u_{\mathrm{mf}})$. That means that the effective heat transfer coefficient due to the mixing of particles approaches 0 as u approaches u_{mf}, i.e. when the fluidization stops and the bed is fixed. Even though the accuracy of the model cannot be assessed within the confines of this thesis, it can at least be shown that the model is consistent with the underlying physical processes.

3.3 Modeling of the tube bundle

The tube bundle model has to describe the shape of the tubes and it has to provide all necessary information to the empirical conduction models of section 3.4. Another requirement on the tube bundle model is that it must not be limited to one specific tube arrangement (e.g. the relative positions of the tubes in the bundle, the shape of the turns, whether the windings are horizontal or vertical, etc. . .) to cover a wide range of regenerator setups.

Developing a single model that meets all these requirements would result in a impractical complex model. Therefore the problem has been solved on the programming level by defining abstract and specialized classes. Since this is mainly a programming issue it is covered in section 5. In this section, the currently implemented model for a staggered tube bundle with horizontal windings is described. Defining additional classes for other cross sections or tube routings that cannot be represented by the models in this section should be very easy.

Figure 6 shows a sketch of a tube bundle with horizontal windings in a fluidized bed box. The turns are made up of a 90° bend with radius r, a straight part and another 90° bend. This path refers to the center of the cross section. Since the tubes are supposed to be cold bent the radius should be chosen so that the resulting bending radius for the inner most tube is larger than $1.5d$.

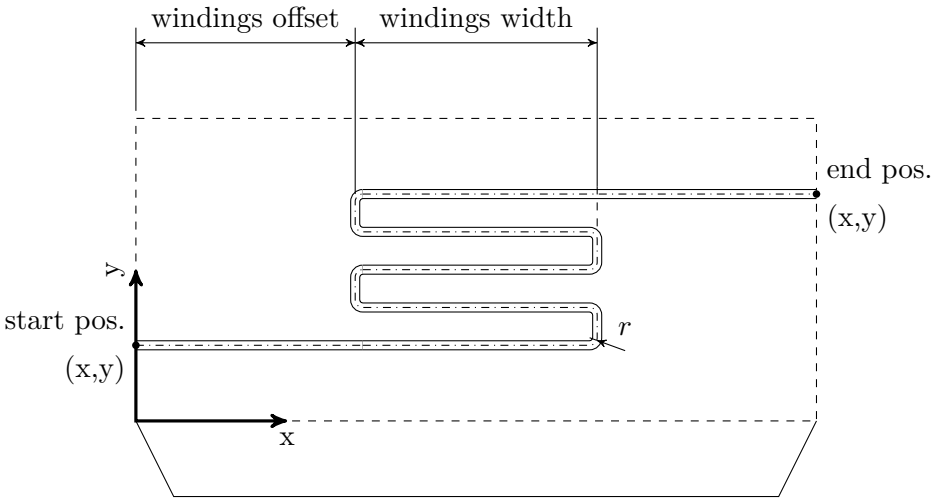

Figure 6: Sketch of a tube bundle with four horizontal turns

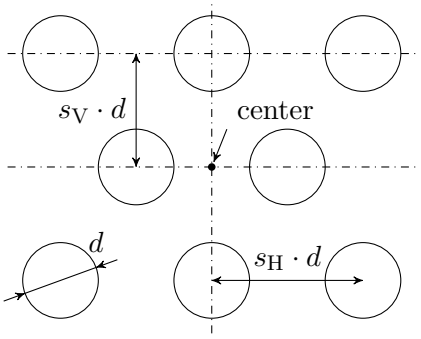

Figure 7: Sketch of the cross section of a staggered tube bundle

A sketch of a staggered cross section, in which eight tubes are arranged in three rows, is shown in figure 7. The relative position of the tubes is controlled by the vertical and the horizontal spacing parameters s_V and s_H.

The information of the tube positioning within the bundle is only intended for conductivity models that take these factors into account. In the simulation the tube bundle is treated as one single tube with equal surface area. The coordinates of the tube bundle elements refer to the center of its cross section (figure 7). The precondition to make this simplification acceptable is that the cross section height is small compared to the winding distance. These factors have to be taken into account when selecting a tube arrangement and the bending radius of the tube bundle.

3.3.1 Flow and heat transfer

The tube bundle is discretized into sections of equal length. The flow is assumed to be friction-less and the thermal processes are modeled quasi-stationary. That means

that the temperature profile in the tube is calculated at every time step but no dynamic effects of the tube flow are taken into account. Under typical operating conditions the heat transfer medium needs around 4s to pass through the regenerator. With a typical simulation time step of 10s the error made by neglecting dynamic flow effects should itself be negligible.

The heat transfer coefficient between heat transfer medium and the tube wall α_{tube} has been calculated with the formulas (4) through (6) in chapter G1 of the VDI-heat-atlas. For these formulas the logarithmic temperature difference $\Delta T_{\ln}$ has to be used.

$$\Delta T_{\ln} = \frac{T_{\text{in}} - T_{\text{out}}}{\ln\left(\frac{T_{\text{tube}} - T_{\text{out}}}{T_{\text{tube}} - T_{\text{in}}}\right)} = \frac{2\Delta}{\ln\left(\frac{T_{\text{tube}} - T_{\text{HTM}} + \Delta}{T_{\text{tube}} - T_{\text{HTM}} - \Delta}\right)} \tag{16}$$

with

$$T_{\text{HTM}} = \frac{T_{\text{in}} + T_{\text{out}}}{2} \qquad \Delta = \frac{T_{\text{in}} - T_{\text{out}}}{2}$$

The logarithmic temperature difference is impractical since it does not allow aggregation of serial heat transfer coefficients with the reciprocal rule. An iterative algorithm would have to be used to calculate the total heat transfer coefficient. Luckily it is easy to show that the logarithmic temperature difference can be approximated by the linear one for sufficiently small tube elements by using the rule of l'Hôpital:

$$\lim_{\Delta \to 0} \Delta T_{\ln} = T_{\text{tube}} - T_{\text{HTM}} \tag{17}$$

3.4 Tube to bed heat transfer

The tube to bed heat transfer is modeled with the tube-bed heat transfer coefficient

$$\alpha_{\text{bed}} = \frac{\dot{Q}_{\text{bed}}}{A(T_{\text{tube}} - T_{\text{bed}})} \tag{18}$$

where $\dot{Q}_{\text{bed}}$ denotes the tube to bed heat flow, A the tube surface area and T_{bed} the bed temperature at a small distance from the tube.

Because of the technical relevance of this heat transfer coefficient numerous research teams have published semi-empirical correlations for α_{bed}. Many of them are described in the Handbook of Fluidization. Furthermore Wesenauer 2015 provides a thorough analysis and comparison of different models.

Although these models generally differ in the modeling approach, their validity range and the value of the estimates some trends are common to all these models (Handbook of Fluidization, section 10.2.2.2):

- The heat transfer coefficient in a fluidized bed is several times higher than the heat transfer coefficient of single phase gas flow or within non-fluidized beds.

- The heat transfer coefficient increases steeply as the fluidization velocity exceeds the minimum fluidization velocity.
- The heat transfer coefficient reaches a maximum at a specific fluidization velocity and then declines slowly.
- The heat transfer coefficient increases with decreasing particle size.

For each tube element the total heat transfer coefficient from the working medium to the fluidized bed α is then calculated with

$$\alpha = \frac{1}{\frac{1}{\alpha_{\text{tube}}} + \frac{1}{\alpha_{\text{bed}}}} \tag{19}$$

The conductivity of the tube wall has been neglected since it is by orders of magnitude higher than α_{bed} and α_{tube}; the heat transfer through radiation has been neglected as well since the temperatures are not expected to exceed 500 °C and radiation effects play only a minor role below that temperature.

3.4.1 Correlations by Martin et. al.

The VDI-heat-atlas proposes to estimate the heat transfer coefficient with the correlations published by Martin 1984.

Martin's correlations are based on an analogy between the particle motion in fluidized beds and the kinetic motion of molecules in gases. The corresponding formulas have been taken from equation (20) through (25) in the VDI-heat-atlas, chapter M5 3.2.

3.4.2 Correlations by Molerus et. al.

Molerus et al. 1995 have developed a correlation for the combined heat transfer coefficient of the gaseous phase and the particles. The formulas were taken from equation (23) through (28) in the Handbook of Fluidization, chapter 10.2.2.2.

These correlations generally produce significantly smaller estimates for the heat transfer coefficient than the correlations of Martin.

3.5 System environment

Though a regenerator of this type can be used in a variety of different processes, only one is considered in this thesis. For the simulations the regenerator is assumed to be used as a superheater in a steam cycle with a Ruth's accumulator. Since the exact temperature-, pressure- and mass-flow-profile of a Ruth's accumulator is very complex and this is not the focus of this thesis, simplified boundary conditions have been used.

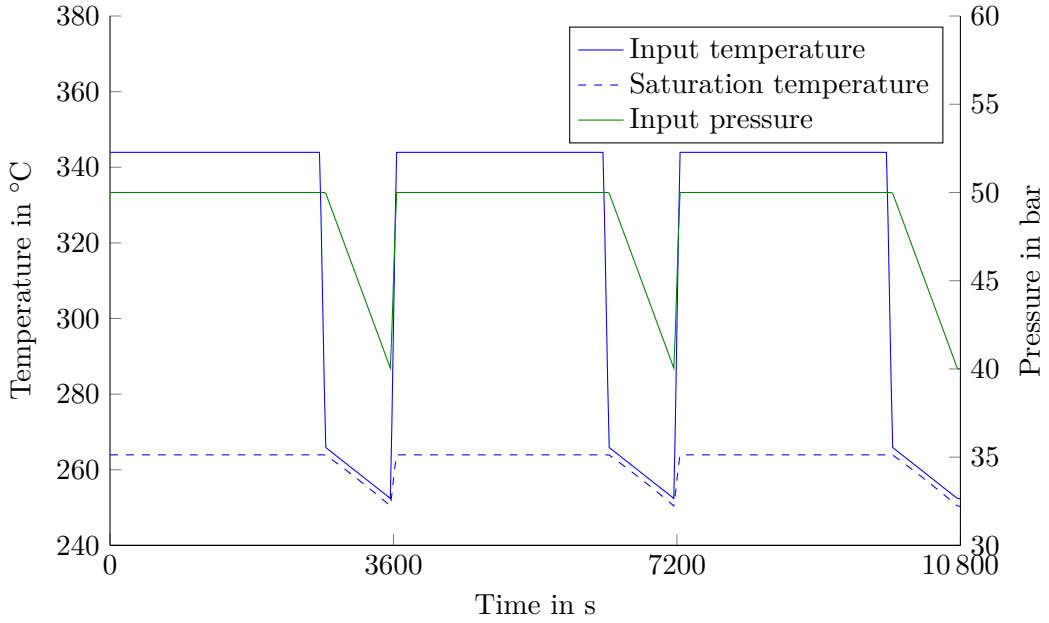

Figure 8: Idealized boundary conditions of the simulation

The heat transfer medium mass flow $\dot{m}_{\mathrm{HTM}}$ is assumed to be constant at all times. During charging the steam enters the regenerator at $T_{\mathrm{superheated}}$ above saturation temperature T_{sat} at nominal pressure p_{N}. During discharging the accumulator keeps the steam mass flow constant by continuously lowering the pressure. It is assumed, that the accumulator lowers the pressure by 20 % and that the steam enters the regenerator at a temperature slightly above saturation temperature T_{sat}. Figure 8 shows an illustration of this process.

Even though the fluidization mass flow (or velocity, or fluidization ratio) can be chosen freely to achieve complex fluidization patterns it has been kept constant in all simulations. The value has been chosen so that specific mean fluidization ratios are realized. Values for each simulation can be found in the corresponding input parameter table in section 6.

To sum up the following boundary conditions are considered in the present regenerator model:

- Heat transfer medium input temperature T_{in}
- Heat transfer medium input pressure p_{in}
- Heat transfer medium mass flow $\dot{m}_{\mathrm{HTM}}$
- Heat transfer medium flow direction
- Either fluidization mass flow $\dot{m}$ or velocity u

4 Analytic reference process

In order to better understand the interactions of the most important model parameters a set of formulas was derived which describe the regenerator as a whole, but are simple enough to be handled analytically. These formulas are also used to estimate model parameters to make the model work as intended.

Of course analytic formulas are not necessary to estimate model parameters in the design phase. One could start with any guess for these parameters and adjust them by running multiple simulations until the regenerator shows the intended behaviour. The problem with this approach is that it requires a lot of computation and time consuming analysis of the results just to get the parameters right, especially if no appropriate starting values are at hand. A more practical way is to describe the system with simplified analytic formulas, use them to derive the required parameters in good approximation and adjust them if necessary. The difficulty is that linear approximations do not suffice due to the complexity of this dynamic system.

In the following calculations of this section only thermal processes are taken into account. The system is assumed to only consist of one box with a single tube of length l. The flow of the heat transfer medium is assumed to be frictionless and dynamic flow effects are neglected. The fluidized bed is modeled as an ideal stirred tank with the temperature T_{bed}; the fluidization is not modeled. The material properties $c_{p,\mathrm{HTM}}$ and $c_{p,\mathrm{particle}}$ as well as the total heat transfer coefficient between heat transfer medium and bed material α are assumed to be constant. For these values an educated guess is required.

Over the course of one cycle with duration τ_{C} the input temperature T_{in} is assumed to be $T_{\mathrm{in,hot}}$ in the beginning and switch to $T_{\mathrm{in,cold}}$ at a certain point. The ratio of the time span where $T_{\mathrm{in}} = T_{\mathrm{in,hot}}$ to the time span where $T_{\mathrm{in}} = T_{\mathrm{in,cold}}$ is referred to as duty cycle δ.

The first two formulas are derived by integrating the tube energy balance over the tube length with the boundary condition $T(x = 0) = T_{\mathrm{in}}$

$$\dot{m} c_{p,\mathrm{HTM}} \mathrm{d}T_{\mathrm{HTM}} = \alpha U (T_{\mathrm{bed}} - T_{\mathrm{HTM}}) \mathrm{d}x \tag{20}$$

$$\Rightarrow T_{\mathrm{HTM}} = T_{\mathrm{bed}} + (T_{\mathrm{in}} - T_{\mathrm{bed}}) \exp\left(-\frac{\alpha U}{\dot{m} c_{p,\mathrm{HTM}}} x\right) \tag{21}$$

and evaluating this formula at $x = l$ when the bed temperature reaches its extreme values:

$$\begin{bmatrix} T_{\mathrm{out,max}} \\ T_{\mathrm{out,min}} \end{bmatrix} = \begin{bmatrix} T_{\mathrm{bed,max}} \\ T_{\mathrm{bed,min}} \end{bmatrix} + \left(\begin{bmatrix} T_{\mathrm{in,hot}} \\ T_{\mathrm{in,cold}} \end{bmatrix} - \begin{bmatrix} T_{\mathrm{bed,max}} \\ T_{\mathrm{bed,min}} \end{bmatrix} \right) \exp\left(-\frac{\alpha A}{\dot{m} c_{p,\mathrm{HTM}}}\right) \tag{22}$$

With this formula a relationship between the input, output and bed temperatures is established.

Once again, the starting point to obtain the formulas that describe the heating and cooling of the fluidized bed is the energy balance. The governing differential equation is just a bit more complex because the temperature profile in the tube has to be taken into account. Using $T(t=0) = T_{\mathrm{bed},0}$ as a generic boundary condition yields

$$m_{\mathrm{bed}} c_{p,\mathrm{particle}} \frac{\mathrm{d}T_{\mathrm{bed}}}{\mathrm{d}t} = \int_0^l \alpha U (T_{\mathrm{HTM}} - T_{\mathrm{bed}}) \mathrm{d}x \tag{23}$$

$$\Rightarrow T_{\mathrm{bed}} = T_{\mathrm{in}} + (T_{\mathrm{bed},0} - T_{\mathrm{in}}) \exp\left(-\frac{t}{\tau_{\mathrm{th}}}\right) \tag{24}$$

where

$$\tau_{\mathrm{th}} = \frac{m_{\mathrm{bed}} c_{p,\mathrm{particle}}}{\dot{m} c_{p,\mathrm{HTM}}} \left[1 - \exp\left(-\frac{\alpha A}{\dot{m} c_{p,\mathrm{HTM}}}\right)\right]^{-1} \tag{25}$$

is the thermal time constant of the system. In contrast to the thermal time constant of the fluidized bed $(m_{\mathrm{bed}} c_{p,\mathrm{particle}})/(\alpha A)$ the thermal time constant of the system as a whole also takes into account the constrictions imposed by the entalpy flow in the tube, which limits the heat that can be transferred to the bed.

The above formulas are evaluated at the end of the heating and the cooling cycle when the bed temperature reaches its extreme value:

$$T_{\mathrm{bed,max}} = T_{\mathrm{in,hot}} + (T_{\mathrm{bed,min}} - T_{\mathrm{in,hot}}) \exp\left(-\frac{\tau_{\mathrm{C}} \frac{\delta}{1+\delta}}{\tau_{\mathrm{th}}}\right) \tag{26}$$

$$T_{\mathrm{bed,min}} = T_{\mathrm{in,cold}} + (T_{\mathrm{bed,max}} - T_{\mathrm{in,cold}}) \exp\left(-\frac{\tau_{\mathrm{C}} \frac{1}{1+\delta}}{\tau_{\mathrm{th}}}\right) \tag{27}$$

Finally one equation to link the required capacity of the regenerator with the bed temperature is required:

$$Q = \overline{P}_{\mathrm{th}} \tau_C \frac{1}{1+\delta} = m_{\mathrm{bed}} c_{p,\mathrm{particle}} (T_{\mathrm{bed,max}} - T_{\mathrm{bed,min}}) \tag{28}$$

with the mean thermal power $\overline{P}_{\mathrm{th}}$.

Equations (22), (26), (27) and (28) can be solved for $\Delta T_{\mathrm{bed}} = T_{\mathrm{bed,max}} - T_{\mathrm{bed,min}}$ when the output temperature difference $\Delta T_{\mathrm{out}} = T_{\mathrm{out,max}} - T_{\mathrm{out,min}}$ and either Q or τ_{th} are given. Inserting the result into the aforementioned formulas yields all unknown temperatures and a very good estimate for the required tube surface area. Based on these values the required bed mass, number of tubes, tube length and the geometry of the bed can be calculated.

The equations derived in this section are based on one single fluidized bed. If an array of n_{box} fluidized bed boxes is to be estimated the formulas have to be adapted accordingly. More specifically instead of the capacity Q and the output temperature variation ΔT_{out} of the whole regenerator the values for a representative bed have to be used.

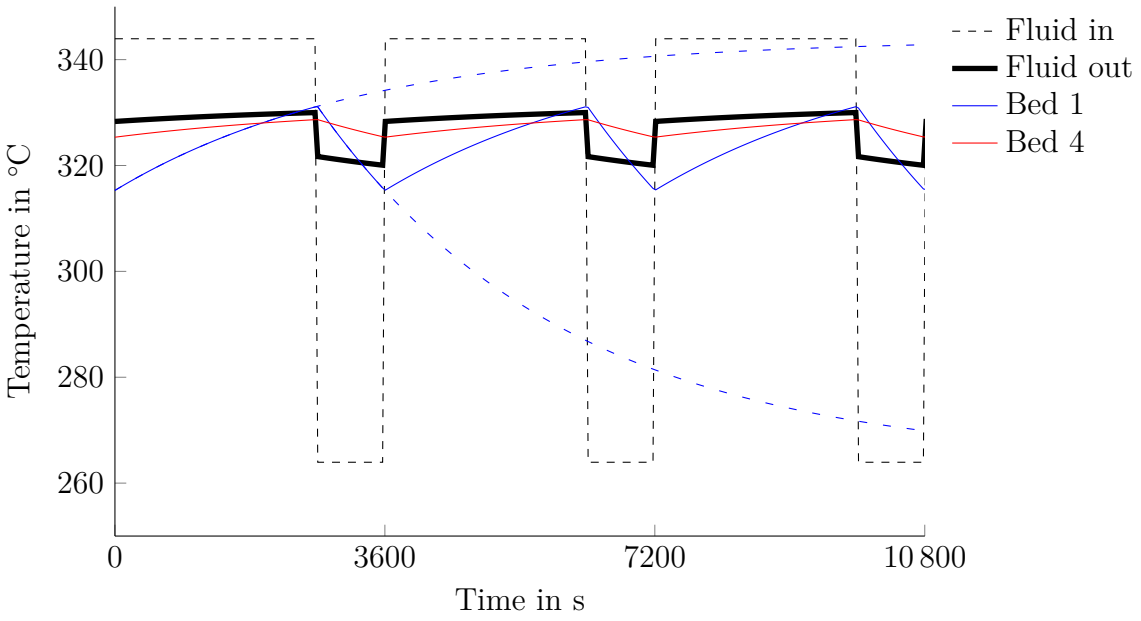

Figure 9: Estimated temperature profile of a regenerator with four boxes

If the flow direction is not reversed during discharging the ratio $\theta = \Delta T_{\text{out,box}}/\Delta T_{\text{in,box}}$ is the same for all boxes in this idealized model. Therefore the values of the first bed can be estimated as follows:

$$\Delta T'_{\text{in}} = \Delta T_{\text{in}} \tag{29}$$

$$\Delta T'_{\text{out}} = \Delta T_{\text{in}}\theta \tag{30}$$

$$Q' = \frac{Q}{\sum_{i=1}^{n_{\text{box}}} \theta^{i-1}} \tag{31}$$

where

$$\theta = \frac{\Delta T_{\text{out,box}}}{\Delta T_{\text{in,box}}} = \left(\frac{\Delta T_{\text{out}}}{\Delta T_{\text{in}}}\right)^{\frac{1}{n_{\text{box}}}}$$

Figure 9 shows the idealized temperature profile of a regenerator with four boxes (e.g. the reference configuration of section 6). The black dashed line represents the assumed input temperature, the black solid line the estimated output temperature according to equation (21). The blue and red lines represent the temperature of the first and the last bed respectively. The blue dashed lines show how the temperature of the first bed would be asymptotically approaching the input temperature according to equation 24 if the input temperature was constant.

Overall the formulas derived above have proven to give good estimates for the design of the regenerator configurations for simulations.

Estimating representative values for when the flow direction is reversed during discharging is more complex due to the interaction of the beds. For values of δ close to 1 the assumption that all boxes store approximately the same amount of heat is viable. The approximation is much more crude than for the operation without flow reversal though.

$$\Delta T'_{\mathrm{in}} = \Delta T_{\mathrm{in}} - \frac{n_{\mathrm{box}} + 1}{2n_{\mathrm{box}}} \left(\Delta T_{\mathrm{in}} - \Delta T_{\mathrm{out}}\right) \tag{32}$$

$$\Delta T'_{\mathrm{out}} = \Delta T_{\mathrm{in}} - \frac{n_{\mathrm{box}} - 1}{2n_{\mathrm{box}}} \left(\Delta T_{\mathrm{in}} - \Delta T_{\mathrm{out}}\right) \tag{33}$$

$$Q' = \frac{Q}{n_{\mathrm{box}}} \tag{34}$$

5 Implementation in Matlab

Matlab is a programming language that is specialized on numerical computing. It is optimized to work efficiently with large data sets like vectors and matrices and provides numerous predefined functions for numerical calculations. To tap into the full optimization potential that Matlab provides much attention has been paid to "vectorize" calculations whenever possible.

In recent releases Matlab also supports object oriented programming. For the implementation of the simulation program an object oriented structure has been chosen because it is more flexible and easier to maintain than traditional Matlab code.

5.1 Class structure

Each component of the regenerator is represented by a class and whenever a component is supposed to be exchangeable abstract classes are used to define a standardized interface. The code for the simulation procedure as well as for the models that require the current state of the regenerator for execution have been put into separate classes to clearly distinguish the physical representation of the regenerator from calculations that describe the regenerator.

The class diagram of the simulation program according to the UML standard[2] is shown in figure 10. Each box represents one class with its name on the top, followed by its properties and the methods at the bottom. The lines between classes represent their dependencies. A filled diamond shape represents a composition relation, e.g. a `FluidizedBed` object contains a `TubeBundle` object. A hollow triangle represents a generalization relation, e.g. `FluidizedBedTemperatureDiffusion` is a kind of `FluidizedBedTemperatureModel`. Lines without symbols represent general associations.

The regenerator is represented by a `FluidizedBedArray` object, which contains a number of `FluidizedBed` objects. At construction the first `FluidizedBed` object has to be passed to the constructor. This object is then replicated and connected in series until the required number of fluidized beds is reached. Apart from the replication method the `FluidizedBedArray` class also provides methods to calculate aggregate values of the properties of the fluidized beds within it (e.g. `totalBedMass`).

Each `FluidizedBed` object contains a `TubeBundle` object and material models for the bed particles and the fluidization medium. The fluidized bed can either operate in mass-flow-controlled, fluidization-velocity-controlled or fluidization-ratio-controlled mode. This behavior is defined by setting the `flowVariable` property to `'u'`, `'mdot'` or `'fluidizationRatio'` respectively. During runtime each `FluidizedBed` also contains references to the corresponding fluidization-, temperature- and bed-tube-conduction-models.

[2] See `https://en.wikipedia.org/wiki/Class_diagram` for more detailed information.

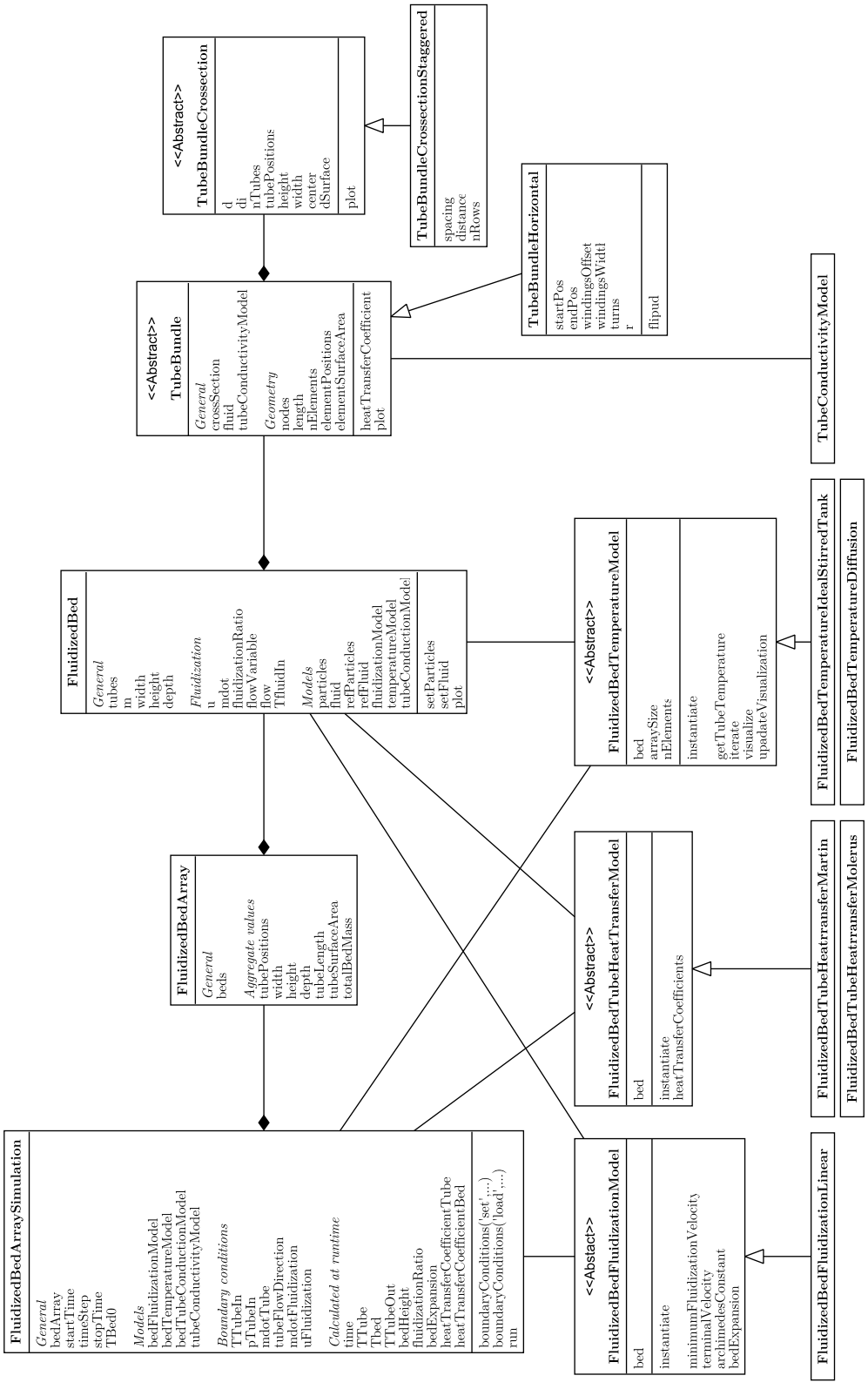

Figure 10: Class diagram of the simulation program

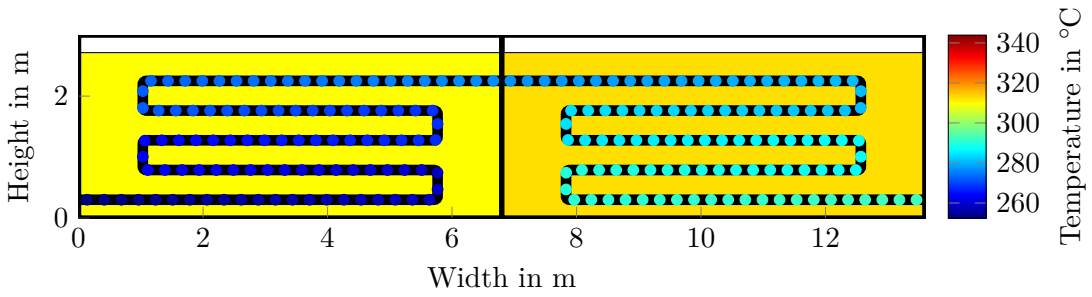

Figure 11: Visualization of the first two boxes of the reference configuration during discharging.

A `TubeBundle` object represents the tubes through which the heat transfer medium flows. The diameter and the positions of the tubes within the tube bundle is determined by a `TubeBundleCrossSection` object. The tube routing is assumed to consist of a series of straight and circular sections without any sharp bends. The coordinates of each section boundary are stored in the nodes property. When the tube is discretized the positions of the tube elements are calculated by interpolating between the nodes with pieces of equal length. During the simulation the tube bundle is treated as if it were one single tube with equal properties.

The `TubeBundle` class is abstract. It provides only the interpolation functions and an interface to the object that calculates the fluid flow within a tube. The `TubeBundleHorizontalTurns` class inherits these functions and provides properties to specify the dimensions of a tube bundle that makes a specific number of horizontal turns within the fluidized bed as shown in figure 6. It issues a warning at construction if there are any geometrical conflicts due to the specified parameters.

The `TubeBundleCrossSection` class is abstract as well. It merely defines a generalized interface for all tube bundle cross sections and provides no additional functionality. Currently only a `TubeBundleCrossSectionStaggered` class is implemented for tube bundles in which the tubes are arranged in a staggered grid (see figure 7). Implementing additional cross sections is very easy and will be especially useful when tube-bed heat conduction models are used that take the tube bundle arrangement into account.

To demonstrate the result of the implementation, figure 11 shows the visualization of a time step, when the regenerator is discharging. The colored area represents the fluidized beds, the black line the pipe routing and the dots represent the temperature of the working medium in the respective tube element.

Besides the classes that represent the physical configuration of the regenerator there are also classes for each calculation model. A super class is implemented for each type of model that defines the interface for the communication with the other classes: `FluidizedBedFluidizationModel`, `FluidizedBedTemperatureModel` and `FluidizedBedTubeConductionModel`. For a detailed description of each of these models see section 3.

Regarding their implementation all these models have in common that they can be created and configured without being associated with a specific `FluidizedBed` object. The coupling is performed afterwards by calling `model.instantiate(fluidizedBed)`. This sequence ensures that the models of all beds are similarly configured and that there is no memory conflict between the model instances for each individual bed. The coupling with the fluidized beds is done automatically by the `FluidzedBedArraySimulation` object in the beginning of the simulation procedure.

One of the most performance critical parts of the simulation is the calculation of the material properties, which is why this task has been heavily optimized. Currently the state variables for all materials are pressure and temperature. Therefore all material models have a `p` and a `T` property and the material properties, for example the density, can be accessed by calling `material.property`. Both the `p` and `T` properties accept value vectors. Then each material property contains a vector with a value for each corresponding (p, T) pair.

Since the `p` and `T` values do not change during each calculation step the material properties can be cached after their first calculation instead of calculating them every time this property is requested. By implementing the caching mechanism on the material model level it is possible to write an efficient simulation code without having to worry if requesting a particular material property at any point in the program will cause unnecessary calculation overhead because it has already been calculated somewhere else before. The cache is cleared whenever the `p` or `T` values are changed.

In the simulations for the present work the material properties of water/steam are calculated based on the formulas in the IAPWS-IF97 release, the tabulated dry air properties are linearly interpolated and the properties of the sand are approximated by polynomials.

A couple of additional classes like `Configurator`, `PostPorcessor` and `ReportGenerator` have been developed which have no influence on the simulation process. They are used to estimate and set simulation parameters, calculate key values from the simulation results and aggregate these key values into tables and diagrams respectively.

5.2 Simulation procedure

The simulation process is started by executing the `run` method of the simulation object after configuring the `FluidizedBedArray` object and its components, initializing the material models, configuring calculation models and setting the simulation parameters. Figure 12 shows flow chart of the simulation procedure according to the UML standard for activity diagrams[3].

[3]Additional information can be found here: `https://en.wikipedia.org/wiki/Activity_diagram`.

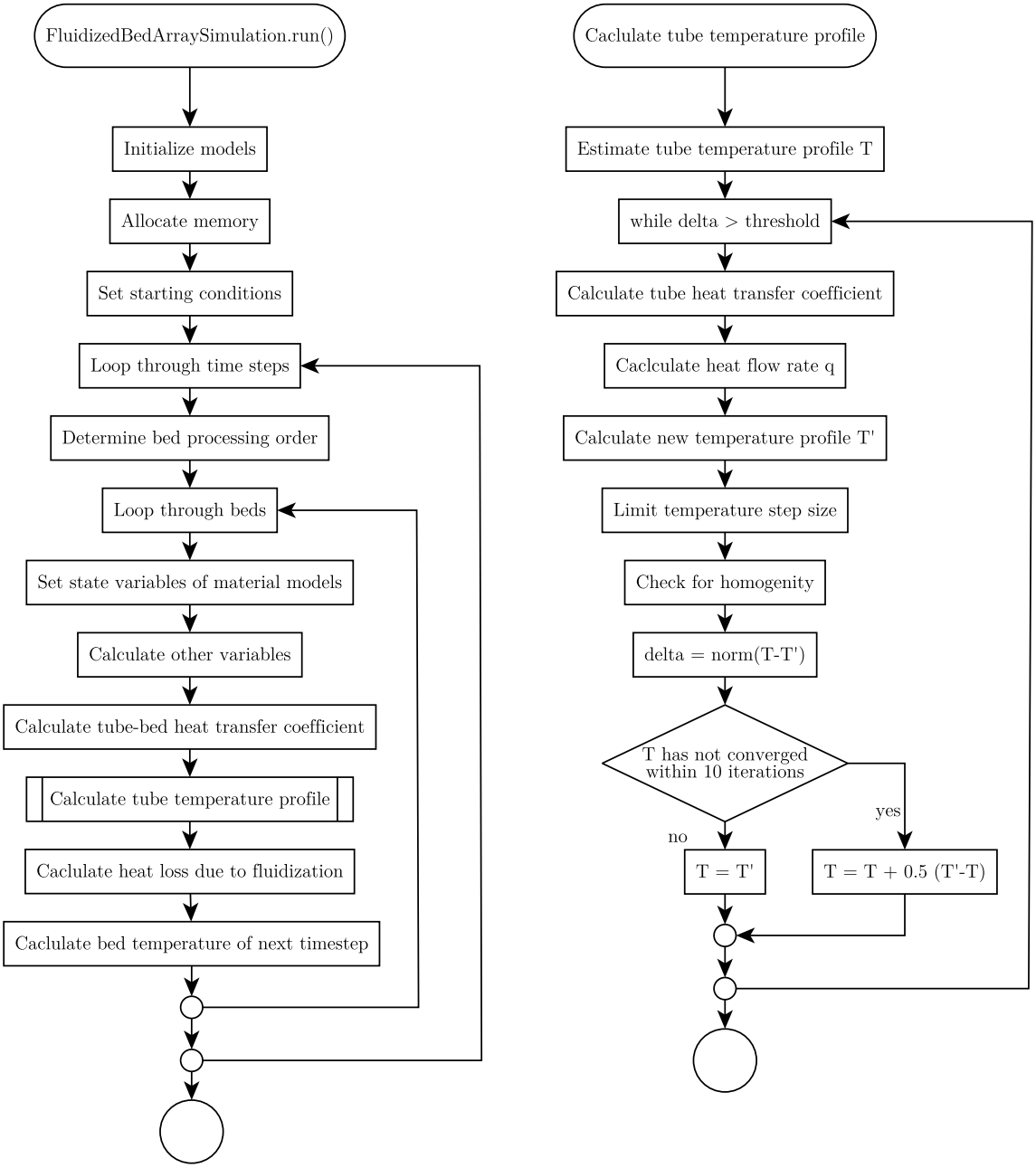

Figure 12: Flow chart of the simulation procedure

First the calculation models are initialized, i.e. coupled to the `FluidizedBed` objects, and memory is allocated for the state variables and the other output variables that are calculated at run time. Then the starting conditions are set.

For the calculation of the bed temperature a fixed step explicit Euler-Scheme is used. Therefore it is possible to determine the time scale beforehand and loop through the time steps in a simple for-loop. Since there is no feedback of any bed to the preceding ones they can be processed sequentially. If the tube flow direction is reversed then the bed processing order has to be reversed as well.

At the beginning of the double loop the (p, T) values of the fluidization medium model and the particle model are set to the corresponding values in the vicinity of each tube element. It is important to do this prior to any calculations because all beds (and also tubes) share the same instances of the material-model-objects. At first this might seem counter intuitive but since the beds are processed strictly sequentially there is no need to keep the data of the other beds in the memory while the calculations of one bed are performed. Also by setting the (p, T) values right at the beginning of each calculation step and not changing them during the calculation it is possible to tap into the full optimization potential of the property caching described in the previous section.

All variables that do not depend on the tube temperature profile, including the tube-to-bed heat transfer coefficient, can already be calculated.

Since the modeling of the tube flow is quasi-static there is no need to solve any differential equations in time to get the temperature profile of tube. Instead an iteration algorithm based on a central difference scheme is used. The initial estimate for the tube temperature profile is calculated with (21). The iteration sequence is shown on the right hand side of figure 12. The following tree mechanisms to improve numerical stability are employed:

1. The maximum temperature step of each node is limited to 1 % of the current bed temperature to prevent the temperature from getting out of range of the material models if the estimated temperature is far away from the true one.

2. If the sign of an element's heat flow changes from one iteration step to the other, i.e. the solution does not converge "homogeneously" the iteration is repeated at least one more time.

3. If the temperature does not converge within the first 10 iterations the cause is usually that the results have started to oscillate. Then the relaxation method with a fixed factor of 0.5 is used to damp the oscillation and make the solution converge.

The iteration stops once the normalized temperature difference between the current and the previous iteration step is below a specified threshold.

With the tube-bed heat flow rate the `iterate` method of the bed temperature model is called to calculate the bed temperature of the next time step. The temperature models and iteration procedures are described in section 3.

This sequence is repeated until the stop time of the simulation is reached.

6 Simulation and Results

For the application as a heat buffer in a steam process the regenerator must prevent the output temperature from exceeding the specified interval to ensure safe operation of the downstream turbine. To achieve this the regenerator has to feature a sufficient heat capacity and rapid heat transfer for dynamic operation while at the same time being as compact as possible. These requirements must be met at the highest possible efficiency and at low cost to justify the implementation of this heat recovery mechanism.

Taking the steam process described in section 3.5 as given, the output temperature variation ΔT_{out} depends mainly on the interaction of the capacity of the regenerator $m_{\text{bed}} c_{p,\text{particle}}$, its time constant τ_{th} from (25) and the heat loss Q_{L}. While the dependence of the size of the regenerator on the bed mass and also of the heat losses and consequently the efficiency on the fluidization mass flow is fairly straight forward, the mechanisms determining the time constant are anything but that.

The main cost drivers are assumed to be the tubes that transport the heat transfer medium, the required particle mass for the beds, the size of the regenerator (material cost and cost of space) and of course the efficiency losses. Some design decisions will have to be made based on cost considerations, especially when difference between two regenerator configurations is irrelevant from a thermodynamic point of view. Even though this thesis does not include any cost estimates the relevant trade-offs are pointed out in the corresponding sections.

To investigate the influence of the design and process parameters listed in table 1 the following analyses have been performed:

Influence of the box aspect ratio
: Whether it is more favorable to build high beds with small base area or low beds with large base area for a given particle volume.

Particle size and conductivity model
: Influence of the mean particle diameter of the bed material and the correlations used to estimate the tube-to-bed heat transfer coefficient.

Trade-off between particle mass and tube surface area
: The same reduction of temperature interval can be achieved with different particle mass to tube surface area ratios. To quantify this trade-off the dynamic factor is introduced.

Bed division and counter flow
: The difference it makes to divide the particle mass on 2/4/8 independent fluidized beds and the effect of flow reversal during discharging.

Changing the fluidization
: Influence of the fluidization mass flow on output temperature variation and efficiency. Is it possible to control the regenerator by changing the fluidization ratio?

Table 1: The input parameters for the simulation with their respective unit and a short description.

Name	Unit	Symbol	
Number of boxes		n_{box}	
Box dimensions	m		width×height×depth
Bed mass	kg	m	Total bed mass
Particle diameter	µm	d_{P}	Mean diameter of bed particles
Tube surface area	m^2	A	Total surface area of the tubes
Fluidization mass flow	kg/s	$\dot{m}$	Fluidization mass flow per box
Fluidization velocity	m/s	u	Superficial velocity of the gas
Counter flow	yes/no	CF	Reversed flow during discharging

Fluidization control

Whether improvements can be achieved by controlling the fluidization conditions.

Finite heat propagation

Comparison of the two temperature models for the temperature distribution in the fluidized beds.

For each analysis separate data series with specific parameter variations have been computed. Each data series is comprised of a number of data sets, which are the results of a simulation run with specific input parameters, i.e. specific regenerator configurations.

Since only a small number of all possible input parameters is varied all regenerator configurations have been derived from one reference configuration, which will be described here in more detail. The reference configuration is part of all data series. In the input and results tables it is marked with an `(R)`.

The reference configuration is a regenerator with four boxes that has been designed to limit the output temperature variation to slightly above 10 K. A sketch of this setup can be seen in figure 1. Each box has the dimensions 6.7 m×3 m×4 m (width×height×depth), is filled with 58 000 kg sand with a mean particle diameter of 100 µm and contains a tube bundle with 24 tubes (d=38 mm) in one row. The tube bundle makes four turns in each box resulting in a total tube length of 110 m and a total surface area of 315.2 m^2.

The mass flow of the heat transfer medium is set to 12 kg/s with a nominal input pressure of 50 bar. The superheated temperature is set to 80 K. The fluidization mass flow has been chosen such that the mean fluidization ratio is approximately 1.5; the bed operates under ambient pressure.

For the estimation of the heat transfer coefficient between the fluidized bed and the immersed tube surface the correlations of Martin have been chosen because they are recommended in the VDI-heat-atlas, which is considered core literature in German speaking countries.

Figure 13 shows the temperature profile of the simulation run with the reference configuration. The vertical dashed lines mark the time points at which the temperature profile over the tube length is plotted in figure 14. The time points are equally distributed over one cycle duration so that the blue line at $t = 6840\,\mathrm{s}$ marks the beginning of the interval that has been used for the calculation of the performance indicators and the purple line at $t = 10\,440\,\mathrm{s}$ marks the end of that interval. For the cycle to be stationary the system has to return to its initial state at the end of the cycle. The lines of the last time point (purple) in figure 14 completely coincide with the lines of the first time point (blue), thereby confirming that the cycle is indeed stationary. Based on the temperature and the mass flow data from this stationary cycle several key values have been calculated which will be described in the following paragraphs.

The fluidization ratio (figure 15) oscillates as a result of the bed temperature variation. In the result tables the mean value over one cycle and all boxes is given.

The difference between the maximum and minimum value of the output temperature during the stationary cycle is referred to as the output temperature variation ΔT_{out}. It has to stay within a specified interval to ensure safe operation of the downstream steam turbine.

The heat flow from the heat transfer medium to the fluidized bed has been calculated via the energy balance of the the heat transfer:

$$\dot{Q}_{\mathrm{bed}} = \left[h(T_{\mathrm{in}}, p) - h(T_{\mathrm{out}}, p)\right] \dot{m}_{\mathrm{HTM}} \tag{35}$$

The extracted heat Q_{E} from the heat transfer medium, released heat Q_{R} to the heat transfer medium and heat loss Q_{L} are then defined as follows:

$$Q_{\mathrm{E}} = \int \dot{Q}_{\mathrm{bed}}\Big|_{\dot{Q}_{\mathrm{bed}}>0} \mathrm{dt} \tag{36}$$

$$Q_{\mathrm{R}} = -\int \dot{Q}_{\mathrm{bed}}\Big|_{\dot{Q}_{\mathrm{bed}}<0} \mathrm{dt} \tag{37}$$

$$Q_{\mathrm{L}} = Q_{\mathrm{E}} - Q_{\mathrm{R}} \tag{38}$$

Integration has been performed with the trapezoid rule. The integration range spans from the start to the end of one stationary cycle. If only the positive or negative values of a function are of interest the integration range has then been adjusted accordingly.

Because energy is a conservative property the heat loss can only take the losses through the system boundary (i.e. due to the fluidization medium) into account. But the second law of thermodynamics states that every energy transformation also results in a loss of energy quality due to irreversibilities of the process. So from a thermodynamic perspective one has to differentiate between useful heat and non-useful heat. To incorporate this distinction into the analysis the exergy flow has been calculated:

$$\dot{E}_{\mathrm{bed}} = \left(h(T_{\mathrm{in}}, p) - h(T_{\mathrm{out}}, p) - T_{\mathrm{U}}\left[s(T_{\mathrm{in}}, p) - s(T_{\mathrm{out}}, p)\right]\right) \dot{m}_{\mathrm{HTM}} \tag{39}$$

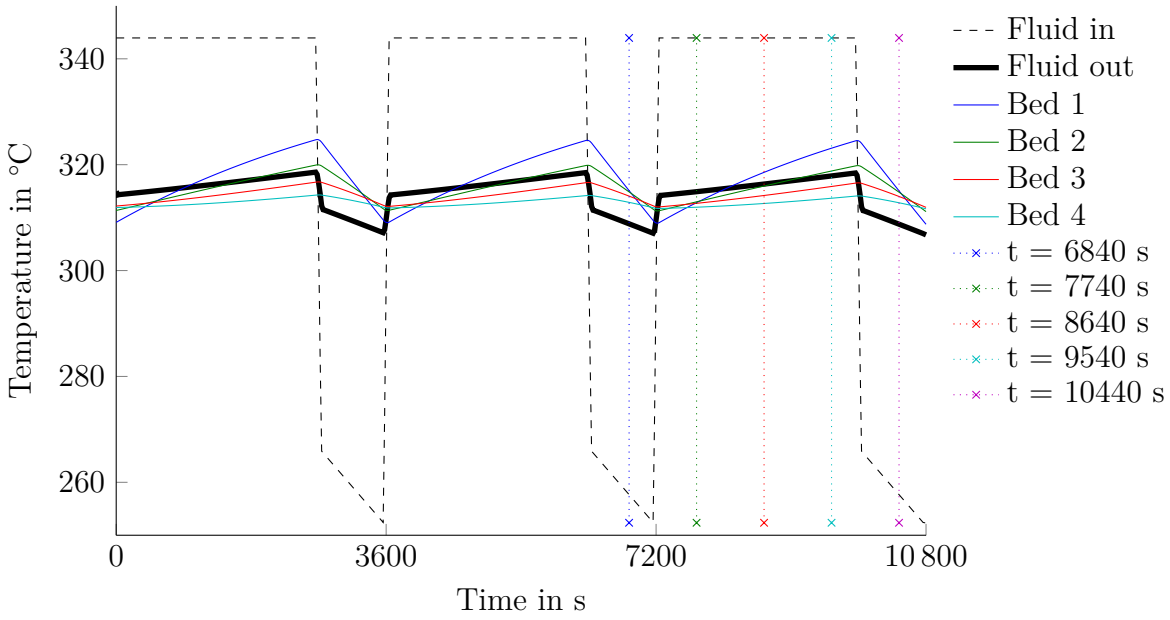

Figure 13: Temperature over time for the reference configuration.

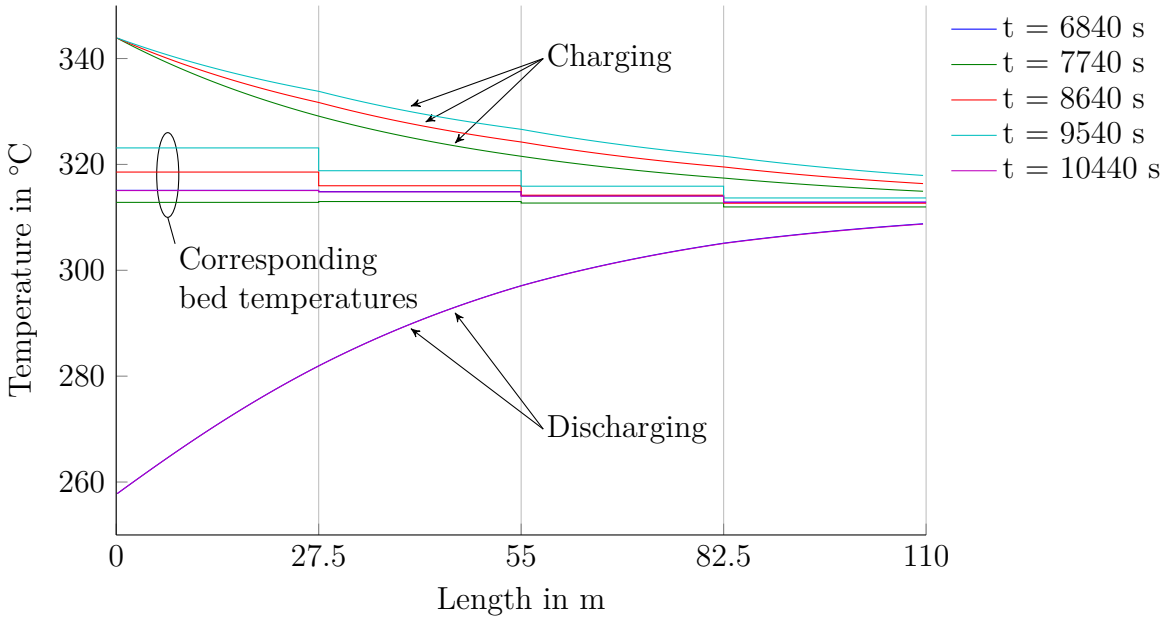

Figure 14: Temperature over the tube length for the reference configuration.

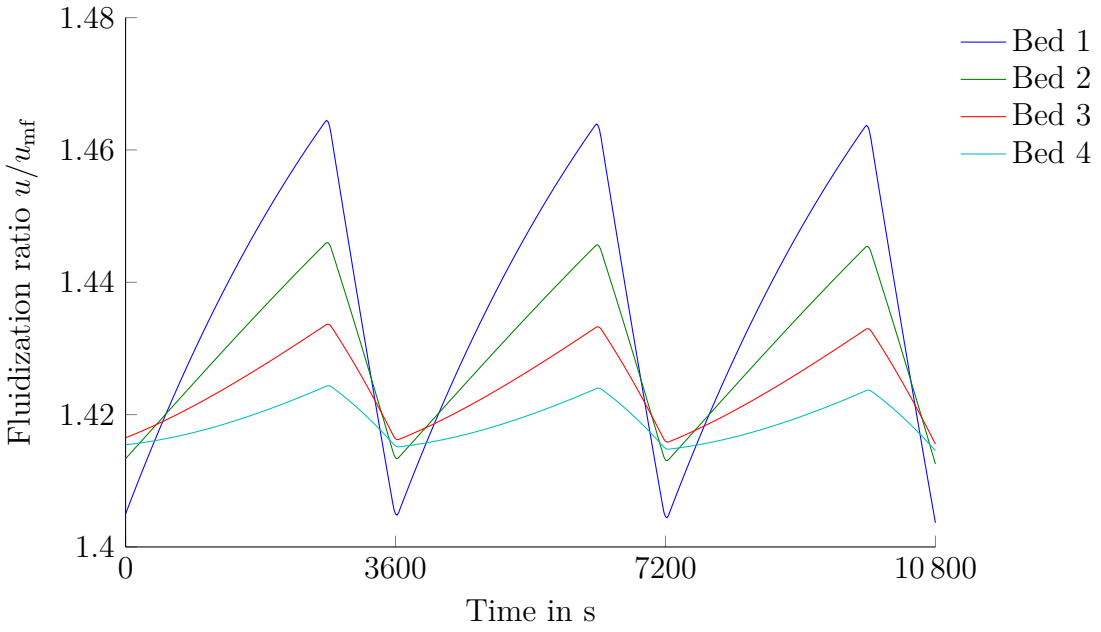

Figure 15: Fluidization ratio over time for the reference configuration.

The corresponding integral values E_{E}, E_{R} and E_{L} have been defined analogously to the integral values of $\dot{Q}_{\mathrm{bed}}$.

The auxiliary work W_{aux} is the work required for compressing the fluidization medium to achieve the required fluidization mass flow. It is calculated by estimating the pressure drop across the fluidized bed, adding an extra 30 % for the nozzle floor and putting this value into the formula for compression work. An isentropic efficency η_{C} of 0.95 has been assumed.

$$\Delta p = (1 - \Psi)(\rho_{\mathrm{particle}} - \rho_{\mathrm{fluid}}) g H_{\mathrm{bed}} \cdot 1.3 \tag{40}$$

$$W_{\mathrm{aux}} = \int \dot{m} c_p \left[\left(\frac{p_{\mathrm{bed}}}{p_{\mathrm{bed}} - \Delta p} \right)^{\frac{\kappa-1}{\kappa}} - 1 \right] \frac{1}{\eta_{\mathrm{C}}} \mathrm{dt} \tag{41}$$

To quantify the heat losses in the regenerator during one cycle the energetic efficiency η_{En} and the exergetic efficiency η_{Ex} have been calculated. The former is a measure for the heat loss due to the mass flow of the fluidization medium whereas the latter also takes the loss of "useful heat" due to the temperature difference during the heat transfer into account.

$$\eta_{\mathrm{En}} = \frac{Q_{\mathrm{R}}}{Q_{\mathrm{E}} + W_{\mathrm{aux}}} \tag{42}$$

$$\eta_{\mathrm{Ex}} = \frac{E_{\mathrm{R}}}{E_{\mathrm{E}} + W_{\mathrm{aux}}} \tag{43}$$

Table 2 summarizes all performance indicators with their respective unit and symbol.

Table 2: Performance indicators with their respective unit and symbol.

Name	Unit	Symbol
Mean fluidization ratio		$\overline{u/u_{\mathrm{mf}}}$
Output temperature variation	°C	ΔT_{out}
Mean output temp.	°C	$\overline{T}_{\mathrm{out}}$
Bed temperature variation	°C	ΔT_{bed}
Mean bed temperature	°C	$\overline{T}_{\mathrm{bed}}$
Extracted heat	kWh	Q_{E}
Released heat	kWh	Q_{R}
Heat loss	kWh	Q_{L}
Auxiliary work	kWh	W_{aux}
Energetic efficiency	%	η_{En}
Exergetic efficiency	%	η_{Ex}
Mean heat transfer coefficient	$\mathrm{W/m^2K}$	$\overline{\alpha}$

Table 3: Input parameters of the simulations on the effect of the box aspect ratio

	m kg	Size m	n_{box}	A $\mathrm{m^2}$	$\dot{m}$ kg/s
Area 20.4 $\mathrm{m^2}$	232 000	27.2 × 4.0 × 3.0	4	315.2	1.13
Area 27.2 $\mathrm{m^2}$ `(R)`	232 000	27.2 × 3.0 × 4.0	4	315.2	1.50
Area 34.0 $\mathrm{m^2}$	232 000	27.2 × 3.0 × 5.0	4	315.2	1.89

6.1 Box aspect ratio

For a given particle mass the aspect ratio of the boxes incorporating the fluidized beds can be varied. The smaller the base area A_{bed}, the higher the boxes have to be. This has an impact on the losses of the regenerator since the fluidization mass flow, which causes the heat loss Q_{L}, is directly proportional to the base area according to $\dot{m} = uA_{\mathrm{bed}}\rho_{\mathrm{fluid}}$ if a specific fluidization ratio is desired. To minimize heat losses the base area should be as small as possible. The auxiliary work W_{aux} on the other hand, which is proportional to the bed height according to (40), exerts a trend in the opposite direction. To minimize it the bed height should be as small as possible. Therefore an optimal box aspect ratio should exist depending on the magnitude and sensibility of the heat loss and the auxiliary work on the box aspect ratio.

To analyze the effect of the aspect ratio the box dimensions have been varied. The fluidization mass flow has been adjusted to achieve similar fluidization ratios; all other parameters have been kept constant. The input parameters are summarized in table 3.

The results in table 4 show that the heat loss in the regenerator is by more than two orders of magnitude higher than the work required to compress the fluidization medium.

Table 4: Results of the simulations on the effect of the box aspect ratio

	$\overline{T}_{\text{out}}$ °C	ΔT_{out} °C	Q_{E} kWh	Q_{L} kWh	W_{aux} kWh	η_{En} %	$\overline{u/u_{\text{mf}}}$	$\overline{\alpha}$ W/m²K
Area 20.4 m²	316	11.3	653	157.7	0.66	75.8	1.43	279
Area 27.2 m² (R)	314	11.4	689	207.1	0.61	69.9	1.43	279
Area 34.0 m²	313	11.4	732	264.6	0.59	63.8	1.43	280

Furthermore the compression work increases only slightly with an increase of the bed height. Therefore it could be argued that the compression work can be neglected when designing the regenerator. Yet one has to keep in mind that the compressor usually runs on electricity which is pure exergy.

To maximize the energetic efficiency of the regenerator, the base area should be kept as small as possible. Since the auxiliary work is negligible the limiting parameter will be the maximum sustainable bed height. The maximum bed height is generally limited due to construction constraints of the boxes and the constructional effort that has to be made to ensure sufficient fluidization over the whole bed height.

6.2 Particle size and conductivity model

Small particles can be fluidized more easily, i.e. at a lower fluidization velocity, than big particles. Since the heat transfer coefficient between the fluidized bed and the immersed tube surface depends mainly on the fluidization ratio similar heat transfer coefficients can be achieved at significantly lower fluidization mass flows. This reduction of the required fluidization mass flow when using smaller particles is expected to reduce the heat loss leading to an increase of the efficiency of the regenerator under similar operating conditions.

To assess the effect of the mean particle diameter of the bed material d_{P} bed materials with three different particle diameters 80 µm, 100 µm and 120 µm have been considered. The fluidization mass flow has been adjusted to achieve similar mean fluidization ratios in all configurations; the tube surface area has been adjusted so that the output temperature variation is similar. Table 5 lists the respective values for each simulation run.

To quantify the impact of the conductivity models from section 3.4 that are used to estimate the heat transfer coefficients between the immersed tube surface and the fluidized bed, the simulations have been run both with the Martin and the Molerus model.

The most striking result of the data listed in table 6 are the severely reduced heat transfer coefficient estimates by the Molerus model. Because the transferred heat, which is the critical parameter for the output temperature variation, is proportional to the product $\overline{\alpha}A$ an increase of the heat transfer area by between 50 % and 80 % has been necessary

Table 5: Input parameters of the simulations on the effect of conductivity model and particle size

	m kg	Size m	n_{box}	A m^2	$\dot{m}$ kg/s
Martin 80 µm	232 000	27.2 × 3.0 × 4.0	4	369.2	0.99
Martin 100 µm (R)	232 000	27.2 × 3.0 × 4.0	4	315.2	1.50
Martin 120 µm	232 000	27.2 × 3.0 × 4.0	4	278.8	2.20
Molerus 80 µm	232 000	27.2 × 3.0 × 4.0	4	566.5	0.99
Molerus 100 µm	232 000	27.2 × 3.0 × 4.0	4	544.4	1.50
Molerus 120 µm	232 000	27.2 × 3.0 × 4.0	4	507.3	2.20

Table 6: Results of the simulations on the effect of conductivity model and particle size

	$\overline{T}_{\text{out}}$ °C	ΔT_{out} °C	Q_{E} kWh	Q_{L} kWh	W_{aux} kWh	η_{En} %	$\overline{u/u_{\text{mf}}}$	$\overline{\alpha}$ $\text{W/m}^2\text{K}$
Martin 80 µm	316	11.4	638	138.5	0.40	78.2	1.47	238
Martin 100 µm (R)	314	11.4	689	207.1	0.61	69.9	1.43	279
Martin 120 µm	312	11.2	766	308.5	0.90	59.7	1.45	320
Molerus 80 µm	316	11.6	639	140.8	0.40	77.9	1.47	155
Molerus 100 µm	314	11.5	688	207.2	0.61	69.8	1.43	161
Molerus 120 µm	312	11.5	765	308.6	0.90	59.6	1.45	175

to achieve similar output temperature variations. Wesenauer 2015 also observes this difference, concludes that the Martin model is grossly over estimating the heat transfer coefficients and recommends to use the Molerus model. Bottom line the quality of the estimates of these correlations seems to vary greatly and without experiments to confirm the real values under the specific operating conditions the simulations should be considered rough trends.

Figure 16 illustrates the fact that the estimations of the two models are in completely different domains highlighting the indispensability of experiments to determine the real heat transfer coefficient in a specific regenerator setup. It also illustrates the sensitivity of the two models to a change of the particle diameter when the fluidization ratio is kept constant. Both models predict an increase of the heat transfer coefficient with increasing particle diameter allowing a reduction of the tube surface area. This effect is much more pronounced when using the Martin model.

The influence of the fluidization mass flow on the energetic efficiency is visualized in figure 17. This reduction of the fluidization mass flow due to the decreased minimum fluidization velocity of small particles led to an increase of the energetic efficiency by 18 percentage points. The graphs for the Molerus and the Martin model coincide because

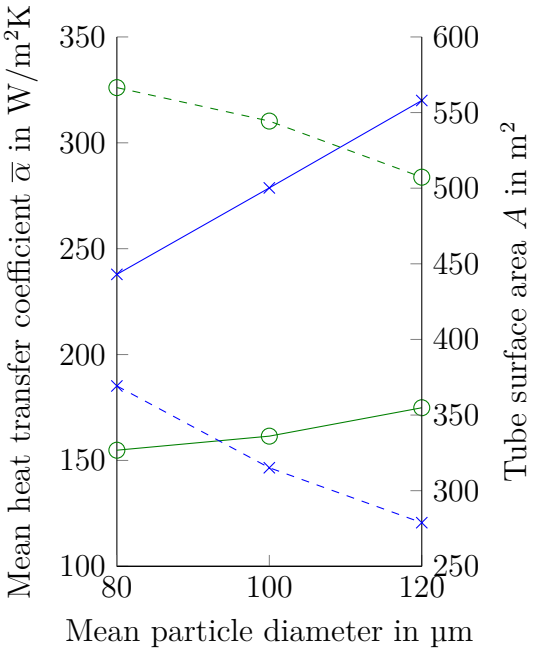

Figure 16: Heat transfer coefficient (solid) and tube surface area (dashed) over particle diameter

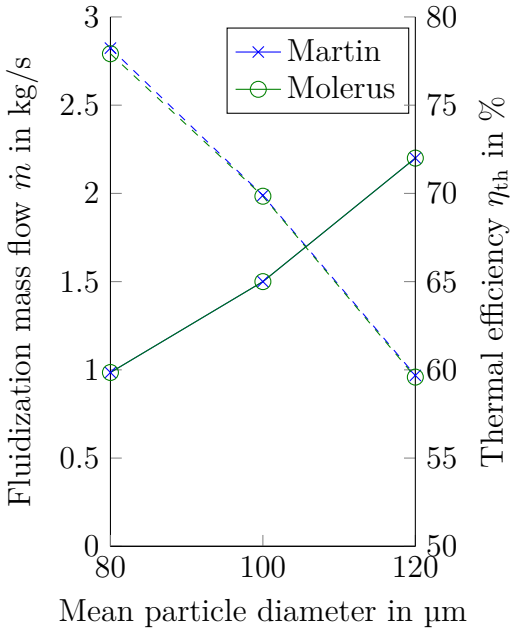

Figure 17: Required fluidization mass flow (solid) and resulting energetic efficiency (dashed) over particle diameter

the heat losses depend only on the temperature profile of the fluidized beds and the fluidization mass flow. Since the tube surface areas have been adjusted to compensate for the different estimates of the heat transfer coefficients, only the mass flow remains as distinguishing factor.

This data series also shows the trade-off between the tube surface area and the mean heat transfer coefficient. Increasing the tube surface area, raises the costs of the regenerator, due to the costs of additional tubes. On the other hand increasing the heat transfer coefficient by increasing the fluidization mass flow, reduces efficiency. From a design perspective it is reasonable to select a fluidization ratio slightly above 1, at which reliable fluidization and sufficiently high heat transfer coefficients can be ensured. This value should of course be confirmed by experiments under similar operating conditions beforehand to avoid nasty surprises due to the obvious inconsistency of the heat transfer coefficient models in the literature.

6.3 Dynamic factor

To stabilize the output temperature in a specific interval, a certain amount of heat has to be "transferred" from the heating to the cooling cycle. This can be achieved by either maintaining a high temperature difference between heat transfer medium and fluidized

bed or by utilizing a big heat transfer area (given that the mean heat transfer coefficient stays constant). The former implies a great particle mass whereas the latter requires longer tubes, i.e. under fixed operating conditions there is a trade-off between particle mass and tube length.

To quantify this trade-off with one number a dimensionless parameter, the dynamic factor, is introduced. It is defined as the ratio of the cycle duration τ_{C} to the energetic time constant of the regenerator τ_{th} as given in (25)[4]. The higher this factor the quicker the bed temperature changes as a response to the temperature of the heat transfer medium. This increases the bed temperature difference ΔT_{bed} and according to the formula $Q = mc_p\Delta T_{\mathrm{bed}}$, less particle mass is needed to store the heat. But, as mentioned before, the heat transfer area has to be increased to compensate for the decreased temperature difference between bed and heat transfer medium in $\dot{Q}_{\mathrm{bed}} = \alpha A(T_{\mathrm{HTM}} - T_{\mathrm{bed}})$.

In terms of configuration parameters the dynamic factor is approximately proportional to A/m, though this would only be true exactly if the temperature change of the heat transfer medium along the tube length was negligible, which of course can never be true in heat buffer applications. Therefore the non-linearities of (25) have to be taken into account, which makes interpretation more difficult. Then the dynamic factor of the regenerator is different from the dynamic factor of the single beds as well.

Even though interpretation of this factor is not straightforward, the dynamic factor has proven to be a useful parameter to distinguish different regenerator setups that limit the output temperature to the same interval, because it is a characteristic value describing the temperature profile of the regenerator. For the analysis in the present work the dynamic factor of the whole regenerator has been calculated.

To study the implications of this factor a number of simulations have been run where the bed mass and the tube surface area have been varied while keeping the output temperature variation as constant as possible. The box size has been adjusted to incorporate the respective particle volume such that the resulting height is 3 m. The fluidization mass flow has been adjusted to achieve similar fluidization ratios. Table 7 summarizes the input parameters to the simulation.

As predicted the bed temperature variation of a regenerator with a low dynamic factor (figure 18) is small. The temperature of the working medium is approaching the bed temperature monotonously over the tube length, resulting in a funnel shaped temperature profile in the space-domain.

In regenerators with a high dynamic factor (figure 19) the bed temperature is considerably more volatile without increasing the output temperature variation. This high volatility causes a complex temperature profile, where at some time points some beds are extracting heat from the working medium while the others are transferring heat to it (time points 8100 s and 10 200 s for example). The result is additional smoothing of the output

[4]For the temperature dependent material properties and the heat transfer coefficient suitable mean values have to be used

Table 7: Input parameters of the simulations on the effect of the dynamic factor

	m kg	Size m	n_{box}	A m^2	$\dot{m}$ kg/s
Dynamic factor 0.7	300 000	34.0 × 3.0 × 4.0	4	303.0	1.90
Dynamic factor 1.0 (R)	232 000	27.2 × 3.0 × 4.0	4	315.2	1.50
Dynamic factor 1.4	166 000	20.0 × 3.0 × 4.0	4	339.3	1.10
Dynamic factor 3.0	92 000	14.0 × 3.0 × 3.5	4	442.5	0.68
Dynamic factor 4.2	84 800	14.0 × 3.0 × 3.0	4	675.0	0.59

Table 8: Results of the simulations on the effect of the dynamic factor

	$\overline{T}_{\text{out}}$ °C	ΔT_{out} °C	Q_{E} kWh	Q_{L} kWh	η_{En} %	$\overline{u/u_{\text{mf}}}$	$\overline{\alpha}$ $\text{W/m}^2\text{K}$
Dynamic factor 0.7	313	11.2	732	270.3	63.0	1.44	282
Dynamic factor 1.0 (R)	314	11.4	689	207.1	69.9	1.43	279
Dynamic factor 1.4	316	11.6	658	152.6	76.8	1.43	279
Dynamic factor 3.0	318	11.5	651	95.6	85.3	1.45	282
Dynamic factor 4.2	318	11.0	677	83.4	87.6	1.47	285

temperature such that the trace appears to be almost sinusoidal (thick black line on the left hand side).

Looking at the results in table 8 it is easy to see that the extracted heat Q_{E} is indeed almost constant in all configurations. The remaining variation can be attributed to the increased heat losses at lower dynamic factors due to the increased fluidization mass flow. Accordingly the efficiency increases significantly with an increase of the dynamic factor.

The bed mass and the tube surface area over the resulting dynamic factor are visualized in figure 20. While the required bed mass falls steeply at low dynamic factors and decreases only slightly at higher dynamic factors, the tube surface area increases slowly at low dynamic factors and steeply towards higher dynamic factors.

In conclusion regenerator configurations with higher dynamic factors seem to be superior to configurations with low dynamic factors in heat buffer applications due to the increased efficiency and the reduced size of the setup. Furthermore the additional smoothing of the output temperature profile in regenerators with high dynamic factors should be beneficial for the downstream steam turbine in terms of thermal stress issues due to the reduced temperature gradient. The limiting factor will be the amount of tubes that can be fit into compact beds as well as the cost for the additional tubes. The optimal dynamic factor could be determined by applying a cost function that takes the cost of particles, tubes, space, compressors, etc. into account.

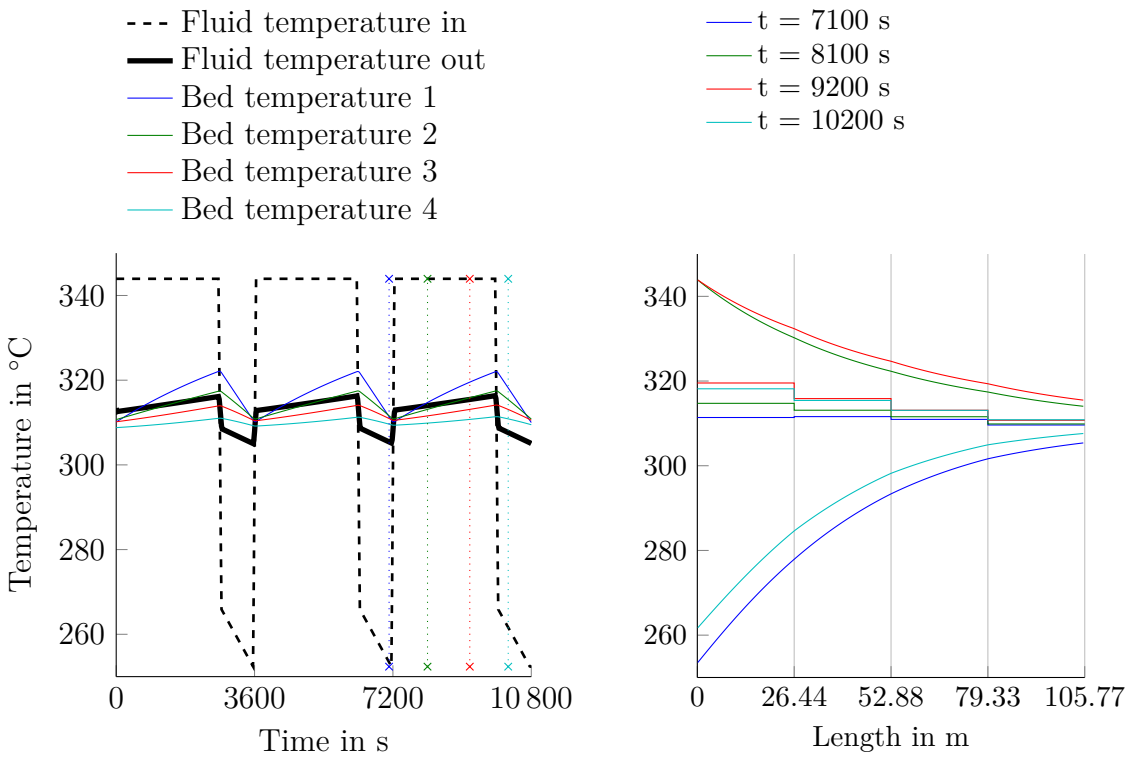

Figure 18: Temperature over time and length with a dynamic factor of 0.7

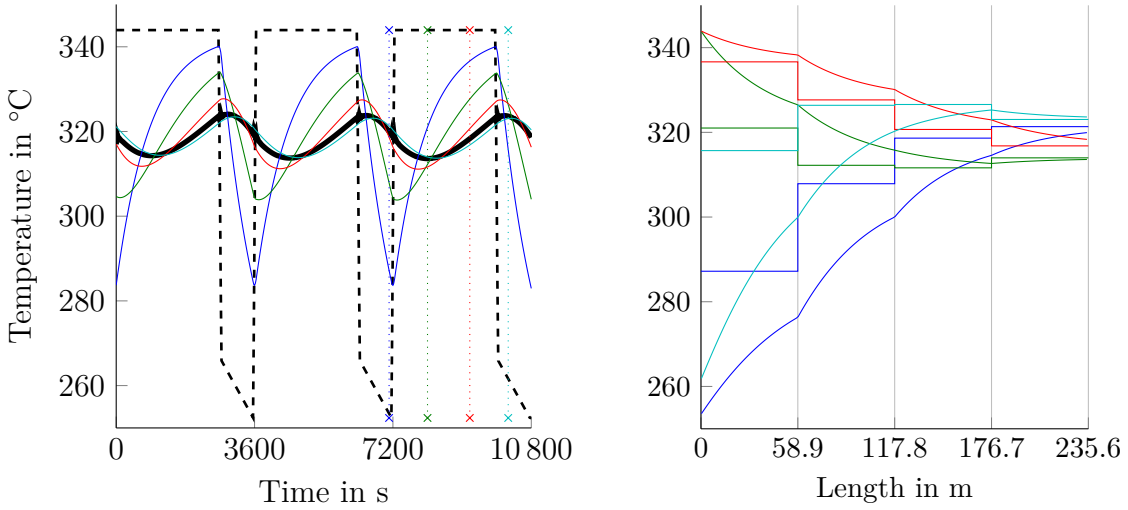

Figure 19: Temperature over time and length with a dynamic factor of 4.2

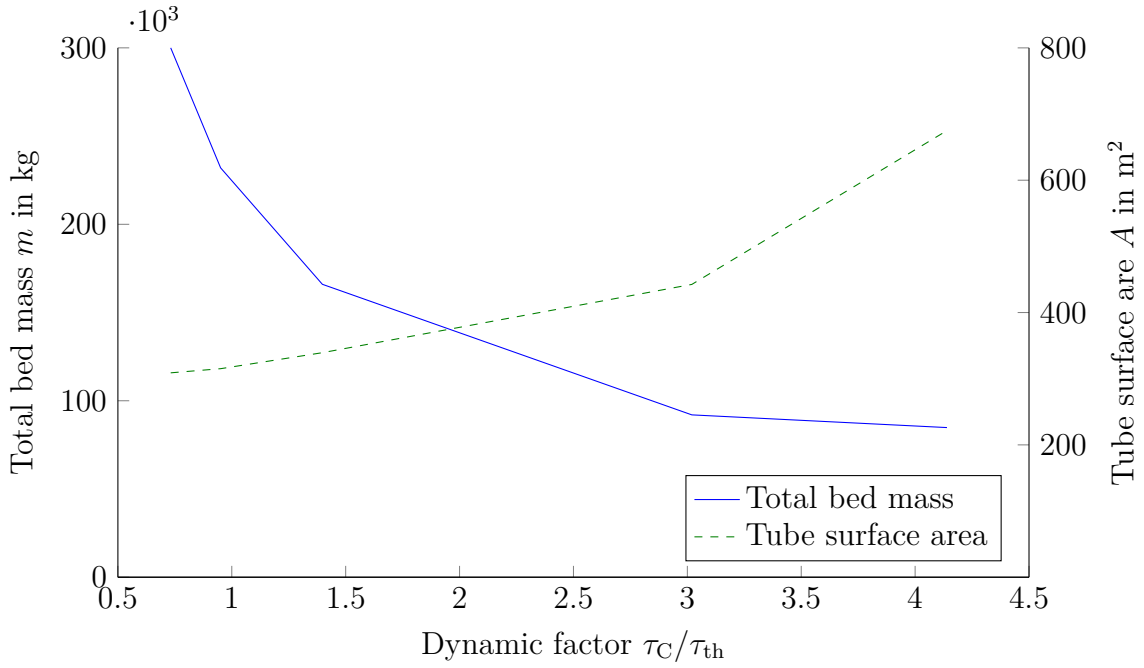

Figure 20: Bed mass and tube surface area over dynamic factor

6.4 Bed division and counter flow

Since thermal processes in the regenerator are anything but linear the division of the bed, i.e. whether the bed mass is distributed over 2, 4 or 8 boxes, is expected to have an impact on its performance. To investigate this effect this data series has been computed where the total bed mass and the total fluidization mass flow has been kept constant while the number of boxes has been varied. To achieve the same output temperature variation, the tube surface area has been adjusted by changing the length of the tubes.

Once at least two beds are connected in series it is possible to change the performance of the regenerator by changing the flow direction during discharging, which is referred to as counter flow (CF). When using CF it is possible to invert the output temperature profile, i.e. to achieve higher output temperatures when the input temperature is low than when the input temperature is high (compare the thick black lines in figure 23 and figure 22). This can be achieved by increasing the heat transfer area sufficiently. The corresponding simulations have been done in the third block of this data series.

The input parameters are summarized in table 9. The mass flow given in the last column of this table is the fluidization mass flow per box. That means that the total fludization mass flow is the same in all configurations, regardless of the number of boxes.

Looking at the temperature profile in figure 21 it is easy to see that the mean bed temperature of the configuration without CF is approximately the same in all four boxes and that the bed temperature variation is declining proportionally to the temperature variation of the heat transfer medium in the respective box. The temperature of the heat

Table 9: Input parameters of the simulations on the effect of the number of boxes and counter flow

	m kg	Size m	n_{box}	A m^2	$\dot{m}$ kg/s
2 boxes without CF	232 000	27.2 × 3.0 × 4.0	2	353.0	3.00
4 boxes without CF (R)	232 000	27.2 × 3.0 × 4.0	4	315.2	1.50
8 boxes without CF	232 000	27.2 × 3.0 × 4.0	8	311.4	0.75
2 boxes with CF	232 000	27.2 × 3.0 × 4.0	2	256.3	3.00
4 boxes with CF	232 000	27.2 × 3.0 × 4.0	4	239.9	1.50
8 boxes with CF	232 000	27.2 × 3.0 × 4.0	8	236.6	0.75
2 boxes with CF inv.	232 000	27.2 × 3.0 × 4.0	2	315.5	3.00
4 boxes with CF inv.	232 000	27.2 × 3.0 × 4.0	4	303.8	1.50
8 boxes with CF inv.	232 000	27.2 × 3.0 × 4.0	8	295.8	0.75

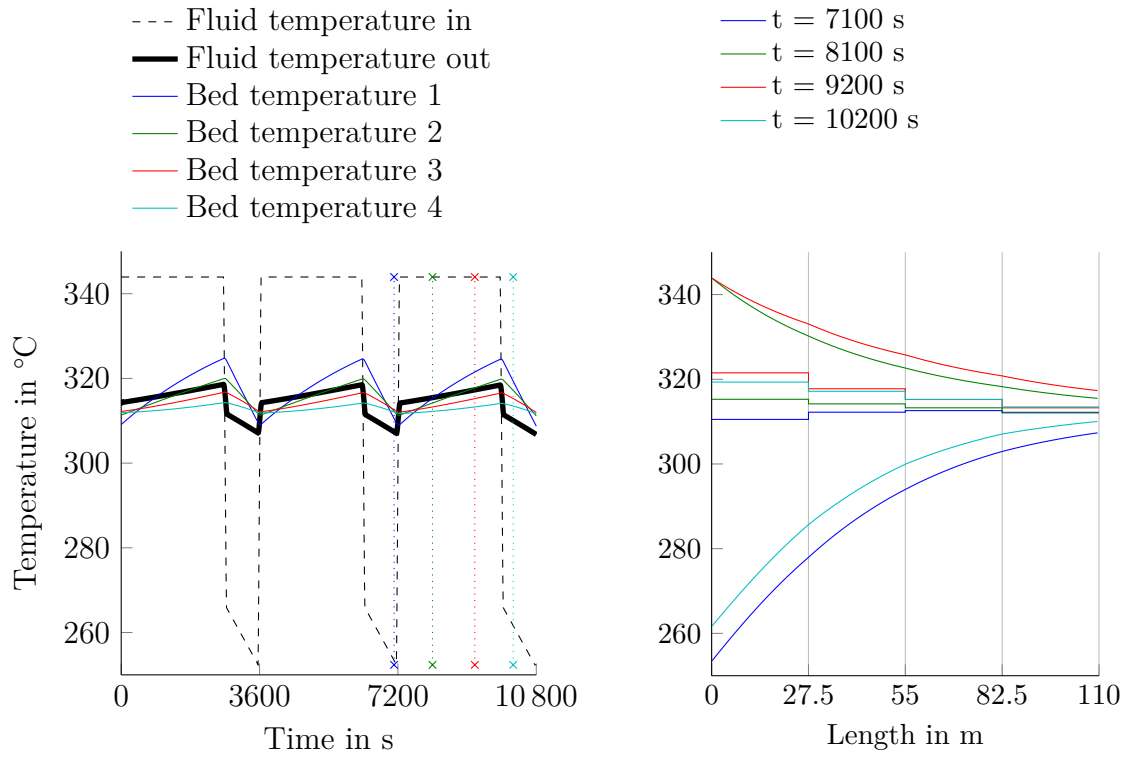

Figure 21: Temperature profile without counter flow

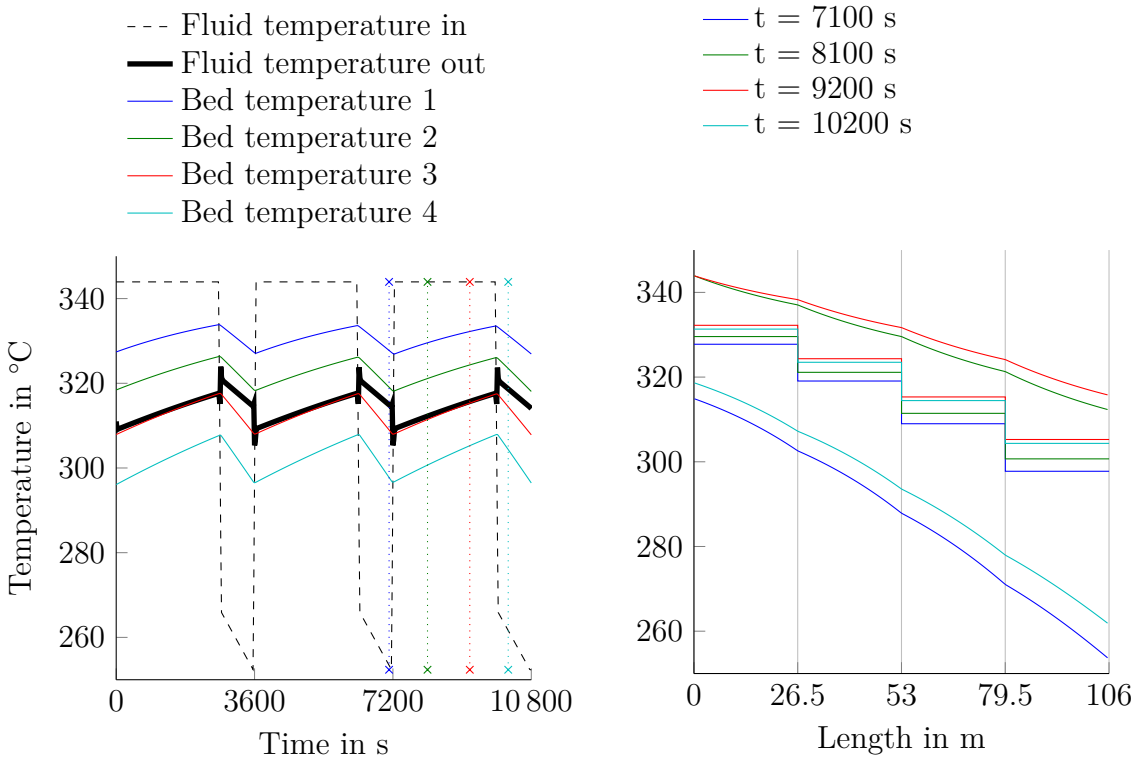

Figure 22: Temperature profile with counter flow and inverted output temperature

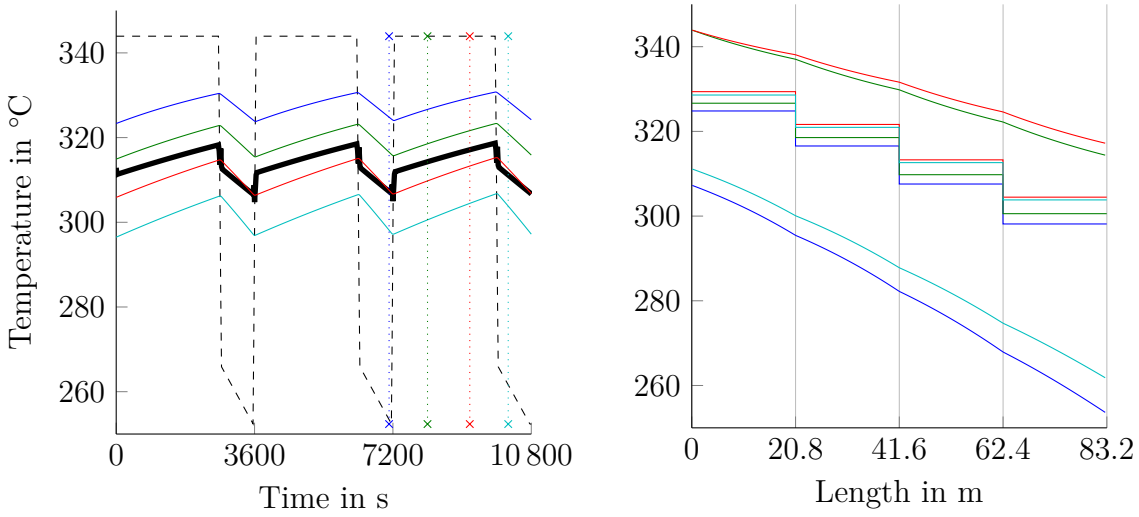

Figure 23: Temperature profile with counter flow

Table 10: Performance indicators for each box without counter flow

	ΔT_{bed} °C	$\overline{T}_{\mathrm{bed}}$ °C	ΔT_{out} °C	$\overline{T}_{\mathrm{out}}$ °C	Q_{E} kWh	Q_{R} kWh	Q_{L} kWh	W_{aux} kWh	η_{En} %	η_{Ex} %
Box 1	15.6	317	57.4	319	307	254	53	0.15	82.8	73.0
Box 2	8.6	316	34.1	317	186	134	52	0.15	72.0	67.2
Box 3	4.6	314	19.8	316	117	66	51	0.15	56.0	53.9
Box 4	2.4	313	11.4	314	80	29	51	0.15	35.8	35.1

transfer medium is converging to the bed temperature monotonously. Since the medium enters the regenerator from the left hand side both during charging and discharging this results in a funnel shaped temperature profile in the space domain.

These trends are also reflected in the numbers in table 10, which lists key parameters for each of the four boxes. The output temperature variations of the single boxes show the constriction tube temperature and the decline of the tube temperature variation. Consequently the energetic efficiency of the boxes declines, because the extracted heat is proportional to the bed temperature variation while the heat losses remain almost constant. In the fourth box the exergetic efficiency is about the same as the energetic efficiency, but in the first box it is significantly lower. This is because the heat transferred from the heat transfer medium to the bed is small compared to the heat loss through the fluidization medium and the smaller temperature difference, at which the heat is transferred in the fourth box compared to the first one.

The temperature profile of the configuration with counter flow in figure 23 shows that the mean bed temperature declines from the left, where the hot medium enters during charging, to the right, where the cold medium enters during discharging. In comparison to the configuration without CF the difference between the bed temperature variations is less distinctive.

Looking at the corresponding numbers in table 11 this temperature profile results in slightly increasing thermal efficiencies from the left to the right hand side, proportional to the bed temperature variations. The reduction of the exergetic efficiency compared to the energetic efficiency is about the same in all four boxes since the temperature difference, at which the heat is transferred, is about the same. An interpretation of the tube temperature variation and mean temperature for each box does not make a lot of sense, since the smoothing of the temperature profile is achieved by all boxes in "teamwork". They have been displayed for consistency with the former table.

There is no qualitative difference between the temperature profile in figure 22 to the one discussed just now other than the fact that the output temperature during discharging is higher than during charging. In table 12 this is reflected by the increased extracted heat value of each box. The increase of extracted heat is also responsible for the increase of the energetic efficiency since the heat losses stayed nearly constant.

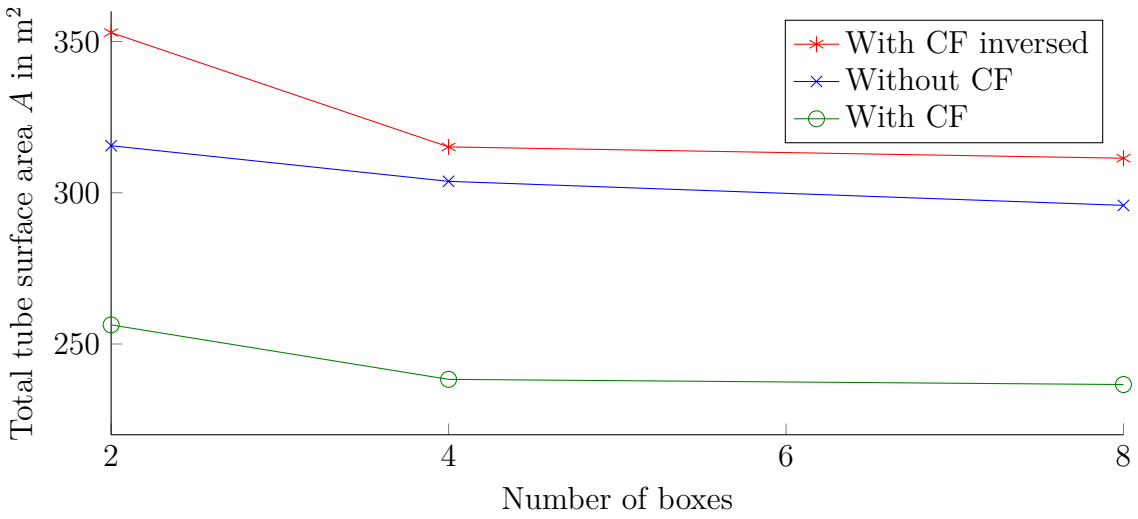

Figure 24: Required tube surface area over number of boxes

Table 11: Performance indicators for each box with counter flow

	ΔT_{bed} °C	$\overline{T}_{\text{bed}}$ °C	ΔT_{out} °C	$\overline{T}_{\text{out}}$ °C	Q_{E} kWh	Q_{R} kWh	Q_{L} kWh	W_{aux} kWh	η_{En} %	η_{Ex} %
Box 1	6.6	328	31.3	330	154	100	54	0.15	65.0	61.0
Box 2	7.5	320	37.3	323	168	114	54	0.15	68.1	63.1
Box 3	8.5	312	44.1	314	185	131	54	0.15	71.0	64.8
Box 4	9.6	302	51.5	305	201	148	53	0.15	73.6	65.9

Table 12: Performance indicators for each box with counter flow and inverted output temperature

	ΔT_{bed} °C	$\overline{T}_{\text{bed}}$ °C	ΔT_{out} °C	$\overline{T}_{\text{out}}$ °C	Q_{E} kWh	Q_{R} kWh	Q_{L} kWh	W_{aux} kWh	η_{En} %	η_{Ex} %
Box 1	6.6	330	28.8	332	154	102	52	0.15	66.1	62.8
Box 2	7.9	322	30.7	324	175	123	52	0.15	70.4	66.1
Box 3	9.5	313	38.4	315	202	150	52	0.15	74.3	68.5
Box 4	11.3	302	47.4	304	230	178	52	0.15	77.3	69.7

Table 13: Results of the simulations on the effect of the number of boxes and counter flow

	$\overline{T}_{\text{out}}$ °C	ΔT_{out} °C	Q_{E} kWh	Q_{L} kWh	η_{En} %	η_{Ex} %	$\overline{u/u_{\text{mf}}}$	$\eta_{\text{Ex}}/\eta_{\text{En}}$
2 boxes without CF	314	11.6	704	210.5	70.0	64.1	1.43	0.916
4 boxes without CF (R)	314	11.4	689	207.1	69.9	63.9	1.43	0.914
8 boxes without CF	314	11.6	691	211.7	69.3	63.3	1.43	0.914
2 boxes with CF	314	11.0	706	210.9	70.1	64.2	1.43	0.916
4 boxes with CF	314	11.4	706	213.9	69.6	63.8	1.43	0.916
8 boxes with CF	314	11.4	706	214.7	69.6	63.7	1.43	0.916
2 boxes with CF inv.	315	−11.1	750	209.4	72.0	66.4	1.43	0.922
4 boxes with CF inv.	315	−11.8	759	208.0	72.5	67.0	1.44	0.924
8 boxes with CF inv.	314	−11.3	762	214.4	71.8	66.3	1.43	0.923

When operating the fluidized bed with CF the part of the output temperature variation that is caused by the sudden change of the input temperature can be eliminated by choosing the optimal tube surface area. At this tube surface area, which is in between the ones of the "CF" and "CF inverted" configuration, the output temperature variation will reach a minimum. The remaining variation will be the one caused by the change of the bed temperature during the heating and cooling cycle. Therefore CF configurations will not benefit in the same way from an increase of the dynamic factor as configurations without CF do, since an increased dynamic factor also always means an increased bed temperature variation. On the contrary: starting from a certain dynamic factor it will be impossible to reduce the output temperature variations to the required value with CF.

The results for the regenerator configurations as a whole in table 13 show that the energetic efficiency of all configurations is about the same. Only the values of the "CF inverted" are slightly higher, but this is not due to a reduction of the heat losses, which are almost exactly the same as in the other configurations, but because of an increase of the transferred heat between the heating and the cooling cycle.

To evaluate these configurations the most relevant parameter is the required tube surface area, that had to be installed to reach the specified output temperature interval. Figure 24 shows the values from table 13 over the number of boxes in a diagram. By operating the regenerator the required tube surface area can be reduced by a remarkable 25 % without an adverse effect on any of the other performance parameters.

Not surprisingly the tube surface area has to be increased significantly to achieve an inversion of the output temperature, making a configuration like this unsuited for real world applications. Nevertheless these simulations show a very interesting aspect of CF that might be worth keeping in mind when developing a control mechanism for the regenerator.

In standard heat exchanger applications CF does increase the exergetic efficiency significantly. Curiously the the exergetic efficiency seems to be unaffected by CF in the simulations. Furthermore any change of the exergetic efficiency seems only to be caused by a change of the energetic efficiency as is shown in the $\eta_{\mathrm{Ex}}/\eta_{\mathrm{En}}$ column. This is despite the fact that the temperature profiles and the efficiency values for the single boxes differ significantly as elaborated before.

In order to better understand the exergetic efficiency in this process it has been derived analytically for an idealized process similar to the one described in section 4.

To calculate the exergy flow as a function of the fluid temperature the entropy difference in (39) has been substituted with the formula for an isobaric process with constant $c_{p,\mathrm{HTM}}$. For a small relative temperature variation along the tube length, i.e. $T_{\mathrm{out}}/T_{\mathrm{in}}$ close to 1 (which is a fairly good approximation in super heaters), the logarithm can be linearized leading to

$$\dot{E}_{\mathrm{bed}} \approx \dot{Q}_{\mathrm{bed}} \left(1 - \frac{T_{\mathrm{U}}}{T_{\mathrm{in}}}\right) \tag{44}$$

Neglecting the auxiliary work and assuming that that the input temperature alternates between a hot and a cold temperature level the exergetic efficiency of the simplified process is given by

$$\eta_{\mathrm{Ex}} = \eta_{\mathrm{En}} \frac{T_{\mathrm{in,hot}}(T_{\mathrm{in,cold}} - T_{\mathrm{U}})}{T_{\mathrm{in,cold}}(T_{\mathrm{in,hot}} - T_{\mathrm{U}})} \tag{45}$$

In the idealized process the exergetic efficiency is directly proportional to the energetic efficiency and the ratio only depends on the temperature spread between charging and discharging and the surrounding temperature. Since no assumptions about the temperature profile in the regenerator had to be made to derive this formula it is valid for operation both with and without counter flow during discharging, explaining why CF does not increase the exergetic efficiency as in continuous heat exchangers.

6.5 Fluidization ratio

During operation the only parameter that can be used to influence the regenerator (considering the input temperature profile as fixed) is the fluidization ratio via the fluidization mass flow. By increasing the fluidization mass flow the mean heat transfer coefficient between the fluidized bed and the immersed tube surface can be increased, but at the same time the heat loss increases as well.

To asses the effect of the fluidization ratio on the operatability and the negative impact on the efficiency of the regenerator this data series has been computed where only the fluidization mass flow has been varied (1.30 kg/s, 1.50 kg/s, 2.10 kg/s, 3.30 kg/s and 5.40 kg/s) to achieve certain fluidization ratios while everything else has been kept constant. The simulations have been run two times: Once with the 4 box configuration

Table 14: Results of the simulations on the effect of the fluidization ratio

	$\overline{T}_{\text{out}}$ °C	ΔT_{out} °C	Q_{E} kWh	Q_{L} kWh	W_{aux} kWh	η_{En} %	$\overline{u/u_{\text{mf}}}$	$\overline{\alpha}$ W/m²K
Fluid. ratio 1.25	315	16.0	641	179.0	0.53	72.0	1.24	229
Fluid. ratio 1.5 (R)	314	11.4	689	207.1	0.61	69.9	1.43	279
Fluid. ratio 2	312	7.1	776	291.6	0.87	62.3	1.99	352
Fluid. ratio 3	307	5.2	912	458.6	1.43	49.6	3.10	410
Fluid. ratio 5	300	4.6	1135	748.8	2.52	33.9	4.99	447
Fluid. ratio 1.25 CF	315	19.1	644	200.0	0.53	68.9	1.24	228
Fluid. ratio 1.5 CF	314	11.4	706	213.9	0.61	69.6	1.43	278
Fluid. ratio 2 CF	312	−12.0	831	302.9	0.87	63.5	1.99	351
Fluid. ratio 3 CF	307	−18.4	993	466.4	1.43	52.9	3.10	409
Fluid. ratio 5 CF	300	−22.2	1236	752.1	2.51	39.1	4.97	446

without CF and once with counter flow. The input parameters to the simulations can be found in table 9 in lines 2 and 5 respectively.

Table 14 shows the results of the simulation runs. When referring to a specific data set the rounded fludization ratio values in the first column are used. The data clearly reflects the trends that have been predicted before: Increasing the fluidization ratio results in an increase of the heat transfer coefficient and the heat loss. The heat losses are the same with and without CF yet the energetic efficiency with CF is slightly higher, because more heat is transferred in total. The work required to compress the fluidization medium increases proportionally to the fluidization mass flow, but is negligible compared to the heat loss.

The results are visualized in figure 25 where the bed temperature variation and the energetic efficiency have been plotted over the fluidization ratio. Without CF both the output temperature variation and the energetic efficiency decline with increasing fluidization ratio. Yet the energetic efficiency declines almost linearly in the considered interval while the output temperature variation features a steep decline at low fluidization ratios and approaches a limit at around 3. If, for whatever reason, the volatility of the input temperature increases it should be possible to keep the output temperature in the specified interval by increasing the fluidization mass flow. In a sense the small output temperature variation is achieved at the price of low energetic efficiency.

This is not (or only to a very small extent) possible in a configuration with CF since the minimum output temperature variation, which is defined by the bed temperature variation, cannot be undercut by increasing the fluidization mass flow. On the contrary: Increasing the fluidization ratio beyond the “optimal” value increases the output temperature variation significantly. From that point on there is so much heat being transferred from the heating to the cooling cycle that the output temperature during heating is actually

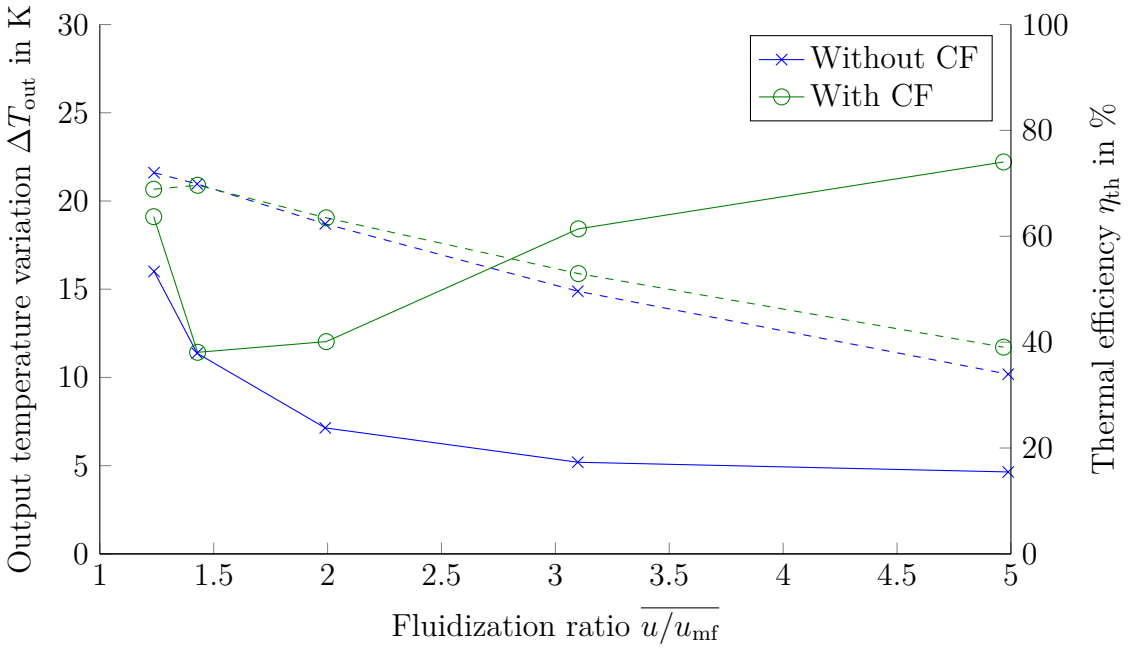

Figure 25: Output temperature variation (solid) and energetic efficiency (dashed) over fluidization ratio

higher than during cooling, i.e. the output temperature is inverted as seen in 22.

Nevertheless the range in which the output temperature can be controlled with CF is significantly bigger than without CF. By developing a sophisticated fluidization control it should be possible to tap into this potential. For example the fluidization could be controlled so that the heat transfer coefficient is low in the beginning of the cycle, when the temperature difference between bed and heat transfer medium is high. Once the bed temperature sinks the fluidization can be increased to keep the heat transfer constant until the end of the cycle. Thereby the output temperature could be stabilized in a very narrow interval.

6.6 Fluidization control

It can usually be assumed with good accuracy that the compressor that compresses the fluidization medium produces a constant mass flow if it is not controlled. Depending on the bed temperature this constant mass flow results in varying fluidization ratios over time as seen in figure 15.

To check whether the efficiency or the operability of the regenerator can be improved by controlling the compressor so that it produces a constant fluidization velocity instead of a constant mass flow this data series has been computed. The superficial velocity of the

Table 15: Results of the simulations on the effect of the fluidization control

	$\overline{T}_{\text{out}}$ °C	ΔT_{out} °C	Q_{E} kWh	Q_{L} kWh	η_{En} %	η_{Ex} %	$\overline{u/u_{\text{mf}}}$	$\overline{\alpha}$ W/m²K
$\dot{m}$-control 1.5 (R)	314	11.4	689	207.1	69.9	63.9	1.43	279
$\dot{m}$-control 3	307	5.2	912	458.6	49.6	45.5	3.10	410
u-control 1.5	314	11.3	690	207.3	69.9	63.9	1.43	279
u-control 3	307	5.2	912	459.1	49.6	45.5	3.10	410

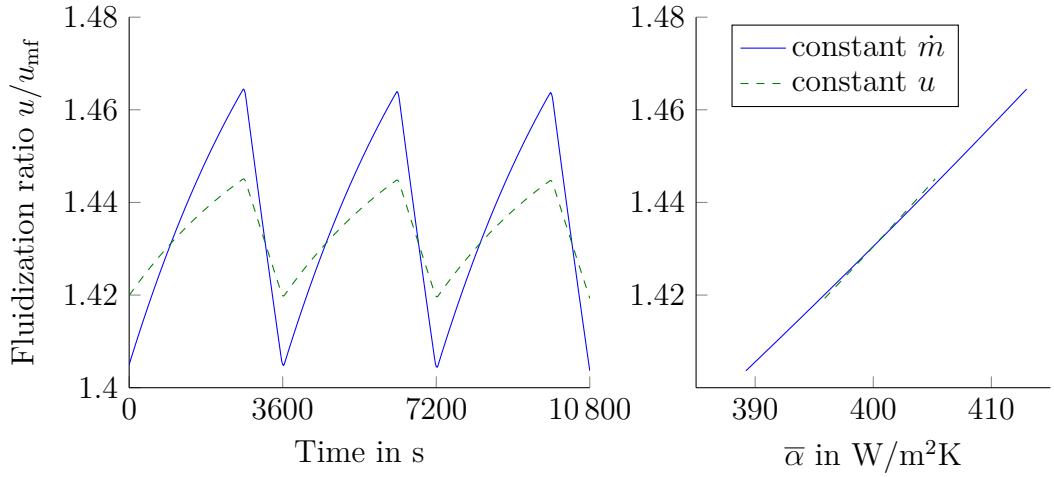

Figure 26: Fluidization rate over time and the mean heat transfer coefficient

control simulations has been chosen such that the mean fluidization ratio is equal to the simulations with constant mass flow.

The simulation results in table 15 show that controlling the compressor does not have an influence on any of the performance indicators.

Evaluation of the fluidization rate over time (figure 26) reveals that the variability of the fluidization ratio and thereby also of the mean heat transfer coefficient can approximately be cut in half by controlling the compressor. The remaining variation can be attributed to the temperature dependence of the minimum fluidization velocity. Since the variation of ±2 % in uncontrolled mode does not have any adverse effects on the effectiveness or the operability of the regenerator, the reduced variability will not be worth the extra effort of measuring the fluidization velocity and controlling the compressor.

6.7 Finite heat propagation

To asses the influence of finite heat propagation within the bed as described in section 3.2.3 the simulation has been run with the diffusion instead of the ideal stirred tank model for

Table 16: Results of the simulations on the effect of temperature propagation in the bed

	$\overline{T}_{\text{out}}$ °C	ΔT_{out} °C	Q_{E} kWh	Q_{L} kWh	η_{En} %	η_{Ex} %	$\overline{u/u_{\text{mf}}}$	$\overline{\alpha}$ W/m²K
Diffusion 1.25	315	16.0	641	179.0	72.0	65.6	1.24	229
Diffusion 1.5	314	11.4	689	207.1	69.9	63.9	1.43	279
Stirred tank 1.25	315	16.0	641	179.0	72.0	65.6	1.24	229
Stirred tank 1.5 `(R)`	314	11.4	689	207.1	69.9	63.9	1.43	279

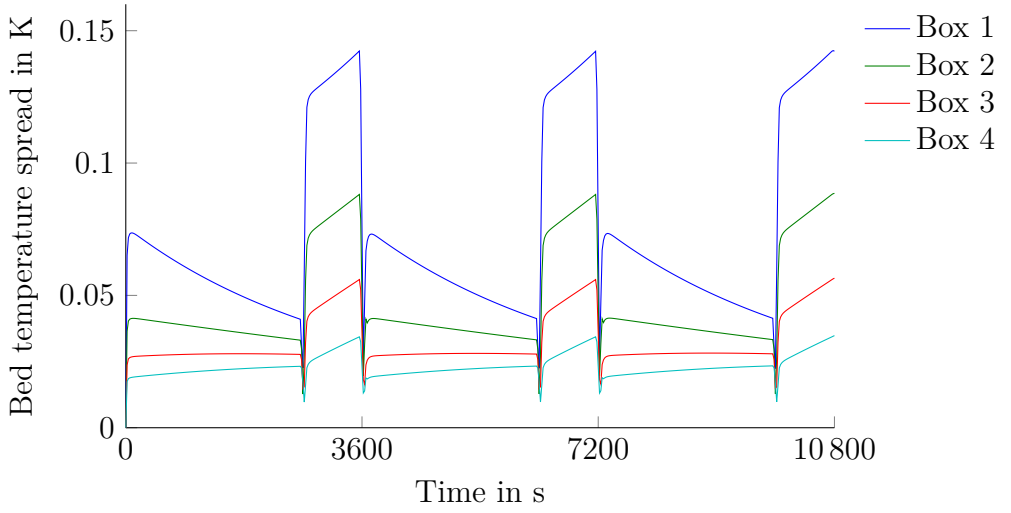

Figure 27: Maximum bed temperature spread across the bed over time

the temperature distribution in the bed.

The simulation has been run with fluidization ratios of 1.25 and 1.5 since the biggest difference is expected at fluidization velocities close to the minimum fluidization velocity.

The results in table 16 show that the finite temperature propagation as estimated by the diffusion model does not have any impact on any of the performance indicators what so ever.

Figure 27 shows the maximum bed temperature spread (i.e. $\max(T_{\text{bed}}) - \min(T_{\text{bed}})$) over time. Although there is a temperature gradient within the bed, that increases sharply when the input temperature changes and decreases slowly afterwards, the deviation stays in the sub-Kelvin range. It comes as little surprise that this does not influence the performance indicators notably.

Although the diffusion model is only a rough estimate for the real temperature distribution of the bed and experiments are needed to back up these results, one can conclude that a fluidized bed does actually behave like an ideally stirred tank. There seems to be no need to make the extra effort and calculate a temperature field for the fluidized bed.

7 Conclusion and Further Steps

First and foremost the simulations have shown that experiments are indispensable, especially to determine the validity of the models used to calculate the heat transfer coefficient between the immersed tube surface and the fluidized bed. Depending on whether the Martin or the Molerus model had been used, the required heat transfer area varied by as much as 80 % (see section 6.2).

Another important finding is, that the work that is required for the compression of the fluidization medium is negligible compared to the heat loss due to the fluidization medium (section 6.1 and section 6.5). Yet it has to be kept in mind that the invested energy is pure exergy.

Since the energy loss due to the entalpy flow in the fluidization medium is directly proportional to the fluidization mass flow, the regenerator setup should be optimized with regard to the reduction of the required fluidization mass flow to achieve the highest possible efficiency. Specifically the simulations have shown that the fluidization mass flow requirement can be reduced by

- operating the beds close to their minimum fluidization point (section 6.5),
- making the fluidized beds "slim", i.e. tall with a small base area (section 6.1),
- using fine particles (section 6.2) and by
- reducing the bed mass and increasing the temperature dynamics (section 6.3).

When the flow direction is reversed during discharging ("counter flow") the required tube surface area, which is a major cost driver, can be reduced by approximately 25 % without adversely affecting any of the other performance parameters, provided that the capacity of the regenerator is sufficient (section 6.4). Because of the minimum capacity requirement counter flow limits the size reduction potential, which can be achieved by increasing the temperature dynamics of the fluidized beds (section 6.3). In other words: The smallest regenerator size can be achieved without counter flow, while regenerators with counter flow require less tubes.

Furthermore, in contrast to continuous heat exchangers, counter flow does not have an impact on the exergetic efficiency (section 6.4). On the other hand the temperature distribution in regenerators with counter flow might offer some interesting optimization potential that can be tapped into by controlling the fluidization mass flow. By reducing the heat transfer in the beginning of the charging and discharging cycle and increasing it towards the end, the output temperature could be stabilized in a much smaller interval.

Apart from developing a control mechanism for the regenerator this simulation model could (and should) also be used to asses the effects of diversions from the ideal periodical input temperature pattern on the output temperature, like for example a change of the duty cycle or a decrease of the "hot"-temperature level.

Regarding the modeling assumptions, the analysis in section 6.7 suggests that the ideal stirred tank assumption is indeed viable and that taking finite heat conduction within the fluidized bed into account is not worth the extra effort. This finding should be backed up by experiments, though.

The weak point of the model, besides the model to calculate the heat transfer coefficients between the fluidized bed and the immersed tube surface, is the model to estimate the fluidization parameters. A model, that is based on the two-phase-theory should increase the accuracy of the simulations. Again experiments will be needed to assess the viability of the fluidization models.

Also incorporating dynamic temperature effects within the heat transfer medium into the simulation, instead of the quasi-static modeling that is used at the moment, should improve its accuracy. Especially,

- when there are high gradients in the input temperature of the heat transfer medium,
- in regenerator configurations with very long tubes,
- and in regenerator configurations where high bed temperature gradients are expected, such as in configurations with a high dynamic factor.

On the other hand including such a model would require a considerable reduction of the simulation time step, since the thermal processes within the heat transfer medium typically take place on a much smaller timescale than the thermal processes of the fluidized bed, which in turn will impact the computation time adversely.

Overall the simulation results suggest that it should be possible to build a regenerator that reduces the temperature variation of the working medium from 85 K to 11 K at a heat transfer medium mass flow of 12 kg/s in a process with a cycle duration of 1 h and a duty cycle of 3. The regenerator would incorporate 92 t particles with a mean diameter of 80 µm in a box with the size 14 m×3 m×3.5 m. The required tube surface area would be 440 m^2. This regenerator would transfer 650 kWh with an energetic efficiency of approximately 90 %.

Especially the high capacity and energetic efficiency should make this technology very attractive in heat recovery application, though it remains to be seen if these values can actually be achieved in real-world realizations of this regenerator. Regardless, further development, e.g. regarding a control mechanism, could reduce the size and material requirements of the regenerator to increase the competitiveness of the fluidized-bed heat regenerator compared to other technologies.

References

Campana, F. et al. (2013). "ORC waste heat recovery in European energy intensive industries: Energy and GHG savings". In: *Energy Conversion and Management* 76, pp. 244–252.

Integrated Pollution Prevention and Control (IPPC) (2013). *Best Available Techniques (BAT) Reference Document for Iron and Steel Production*.

Integrated Pollution Prevention and Control (IPPC) (2014). *Reference Document on Best Available Techniques in the Ferrous Metals Processing Industry*.

International Energy Organization (2010). *Energy technology perspectives*.

Izquierdo-Barrientos, M.A. et al. (2013). "Thermal energy storage in a fluidized bed of PCM". In: *Chemical Engineering Journal* 230, pp. 573–583.

Johansson, Maria T. et al. (2014). "Electricity generation from low-temperature industrial excess heat — an opportunity for the steel industry". English. In: *Energy Efficiency* 7.2, pp. 203–215. ISSN: 1570-646X.

Luo, Kun et al. (2015). "CFD–DEM study of mixing and dispersion behaviors of solid phase in a bubbling fluidized bed". In: *Powder Technology* 274, pp. 482–493.

Martin, Holger (1984). "Heat transfer between gas fluidized beds of solid particles and the surfaces of immersed heat exchanger elements, Part II". In: *Chemical Engineering and Processing: Process Intensification* 18.4, pp. 199–223.

Molerus, O et al. (1995). "Particle migration at solid surfaces and heat transfer in bubbling fluidized beds — II. Prediction of heat transfer in bubbling fluidized beds". In: *Chemical Engineering Science* 50.5, pp. 879–885.

Mostafazadeh, Majid et al. (2013). "Numerical analysis of the mixing process in a gas–solid fluidized bed reactor". In: *Powder Technology* 239, pp. 422–433.

Verein Deutscher Ingenieure (2013). *VDI-heat-atlas (Ger: VDI-Wärmeatlas)*. Springer Berlin Heidelberg. ISBN: 9783642199806.

Wesenauer, Florian (2015). "Wärmeübergang von blasenbildender Wirbelschicht zu Rohrbündel-Wärmetauscher". Vienna University of Technology.

Yang, W.C. (2003). *Handbook of Fluidization and Fluid-Particle Systems*. Chemical Industries. Taylor & Francis. ISBN: 9780203912744.

List of Symbols

A	Total tube surface area
A_{bed}	Bed base area
Ar	Archimedes number
α	Heat transfer medium to bed heat transfer coefficient
$\overline{\alpha}$	Mean heat transfer medium to bed heat transfer coefficient
α_{bed}	Tube to bed heat transfer coefficient
α_{tube}	Heat transfer medium to tube wall heat transfer coefficient
CF	"Counter flow"; Whether the flow direction of the working medium is reversed during discharging
$c_{p,\text{HTM}}$	Specific isobaric heat capacity of the heat transfer medium
$c_{p,\text{particle}}$	Specific isobaric heat capacity of a bed particle
d_{p}	Mean particle diameter
δ	Duty cycle of the slab casting process
$\dot{E}_{\text{bed}}$	Exergy flow from the heat transfer medium to the bed
E_{E}	"Extracted exalpy"; Heat transferred from the heat transfer medium to the bed during one cycle
E_{L}	Exergy loss during one cycle
E_{R}	"Recovered exergy";Heat transferred from the bed to the heat transfer medium during one cycle
H_{bed}	Bed height
g	Gravity constant
$h(T, p)$	Entalpy at the specified temperature and pressure
η_{En}	Energetic efficiency of the regenerator
η_{Ex}	Exergetic efficiency of the regenerator
κ	Heat capacity ratio of the fluidization medium
k_x	Effective horizontal heat conductivity of the bed
k_y	Effective vertical heat conductivity of the bed
$\dot{m}$	Fluidization mass flow (per box)
m	Bed mass of all beds
m_{bed}	Bed mass
$\dot{m}_{\text{HTM}}$	Heat transfer medium mass flow
n_{box}	Number of fluidized bed boxes in the regenerator
ν_{fluid}	Dynamic viscosity of the fluidization medium
Δp	Pressure drop across the bed
p_{bed}	Pressure within the fluidized bed
p_{in}	Input pressure of the working medium
Δp_{N}	Normalized pressure drop across the bed
p_{N}	Nominal pressure of the working medium
Ψ	Bed expansion
Ψ_{mf}	Bed expansion at minimum fluidization
$\dot{Q}$	Heat flow

Q	Capacity of the regenerator
$\dot{q}$	Specific heat flow per volume
$\dot{Q}_{\text{bed}}$	Heat flow from the heat transfer medium to the bed
Q_{E}	"Extracted heat"; Heat transferred from the heat transfer medium to the bed during one cycle
Q_{L}	Heat loss during one cycle
Q_{R}	"Released heat"; Heat transferred from the bed to the heat transfer medium during one cycle
ρ_{particle}	Density of bed particle
ρ_{fluid}	Density of fluidization medium
$s(T, p)$	Entropy at the specified temperature and pressure
T_{HTM}	Temperature of the heat transfer medium
T_{bed}	Bed temperature
ΔT_{bed}	Bed temperature variation
$\overline{T_{\text{bed}}}$	Mean bed temperature
$(Tc_p)_{\text{fluid,in}}$	Entalpy of fluidization medium when entering through the bottom of the bed
$(Tc_p)_{\text{fluid,out}}$	Entalpy of fluidization medium when exiting at the top of the bed
T_{fluid}	Fluidization medium temperature
T_{in}	Input temperature of the heat transfer medium
$T_{\text{in,cold}}$	Input temperature of the heat transfer medium during discharging
$T_{\text{in,hot}}$	Input temperature of the heat transfer medium during charging
T_{out}	Output temperature of the heat transfer medium
ΔT_{out}	Output temperature variation
$\overline{T_{\text{out}}}$	Mean output temperature
T_{sat}	Saturation temperature of the heat transfer medium
$T_{\text{superheated}}$	Excess temperature of the heat transfer medium above its saturation temperature
t_{T}	Bed turnover time
T_{U}	Ambient temperature
T_{wall}	Temperature of the tube wall
τ_{C}	Cycle duration of the slab casting process
τ_{th}	Thermal time constant of the regenerator
U	Tube circumference
u	Superficial gas velocity of the fluidization medium
u_{T}	Superficial gas velocity at which the bed enters the tubular regime
u_{mf}	Superficial gas velocity to achieve minimum fluidization
$\overline{u/u_{\text{mf}}}$	Mean fluidization ratio
V_{bed}	Volume of the bed
$V_{\text{particles}}$	Volume of the bed particles
W_{aux}	Auxiliary work
W_{bed}	Bed width

List of Figures

List of Tables